MASTERARBEIT

„Mixing of different water masses and its effect on prokaryotic and viral communities"

Carl Philip Kruspe, BSc

angestrebter akademischer Grad:

Master of Science (MSc)

Wien, 2012

TABLE OF CONTENTS

ABSTRACT

Viruses are the most abundant biological entity on the planet. In this study, we addressed the question whether mixing of water masses has an impact on prokaryotic and viral community composition, the frequency of virally-infected cells (FIC), and viral production (VP). Therefore prokaryotes from three different water masses were obtained from the North Atlantic and incubated in 2 incubation experiments with 7 different treatments for up to 72 h. Prokaryotic and viral abundance were determined using a flow cytometer. Prokaryotic and viral community composition were determined using PCR-based fingerprinting methods. Inter-experimental trends for FIC and VP were revealed for prokaryotes of the North Atlantic Deep Water (NADW) when incubated either in Mediterranean Sea Overflow Water (MSOW) or Antarctic Intermediate Water (AAIW). Mantel tests showed in both experiments that the bacterial community composition was only weakly influenced by the treatment effects, as well as the viral community detected with the primer CRA-22. In contrast, the treatments influenced archaeal community composition as obtained by the archaeal reverse primer and viral community composition detected by the primer OPA-13. The results indicate that mixing of water masses has a stimulating effect on FIC and VP of prokaryotes originating from NADW when incubated in MSOW or AAIW.

1. INTRODUCTION

1.1 Viruses in the sea

Despite the controversial discussion whether viruses are living organisms, viruses are the most abundant biological entity on Earth with an estimated total number of 10^{31} viral particles in the biosphere (Edwards & Rohwer, 2005; Suttle, 2007). Viruses (size of 20 – 200 nm) containing 0.2 fg of carbon sum up to 200 Mt of carbon in the ocean and would be equivalent to the carbon in ~75 million blue whales (Suttle, 2005). Nevertheless this is only 5 % of total prokaryotic biomass. Viruses are obligate parasites and are not able to replicate outside their host (Roossinck, 2011). Therefore virally-infected organisms range from *Bacteria* and *Archaea* to all kinds of eukaryotes (Munn, 2006). Viruses have several different life cycles: lytic, lysogenic, pseudolysogenic, and chronic infections (Weinbauer, 2004). During the pseudolysogenic life cycle, the viral genome is in an unstable state within the host cell since it does not integrate into the host genome. The pseudolysogenic life style appears to be a strategy of viral survival in starved host cells. Chronically infected host cells release the viral progeny constantly without lysing. Once the viral chromosome has been injected into the host cell during the lytic or virulent cycle, the host chromosome will break down and the expression of the viral genes begins, leading inevitably to cell lysis and the release of progeny viruses. Unlike virulent bacteriophages (greek for 'bacteria eater'), lysogenic viruses integrate their genome into the host chromosome without lysing the cell and the so-called prophage prevails until inducing agents like UV-radiation alter the cycle towards the lytic pathway. After assembly, the progeny phages are released via cell lysis.

The burst size (BS) is the number of viruses released per lysed prokaryotic cell and ranges from 4 in freshwater systems to 300 in marine ecosystems (Parada *et al.* 2006). In addition to the morphotype and possible hosts for infection, genomic information is used for taxonomical classification of viruses. Viruses are distinguished by single (ss) or double-stranded (ds) DNA as well as RNA (Ackermann, 2003) and according to the International Committee on

Taxonomy of Viruses (ICTV), there are currently (2011) six established orders which split up into several families and subfamilies.

1.2 Interactions of prokaryotes and viruses

For successful infections, it is crucial for viruses to maximize encounter rates with compatible hosts since they do not have the ability of active locomotion. Thus, with increasing cell numbers, the chance for viral attachment onto the surface of a host cell will increase as well. According to Suttle (2005), Weinbauer (2004), and Hendrix *et al* (1999) viral genetic diversity is very high. Unlike ribosomal RNA in cellular organisms, there is no universal gene present in all viruses complicating taxonomic classifications. Nevertheless, it is widely assumed that viruses are strain-specific in terms of their hosts (Wommack & Colwell, 2000; Rodriguez-Valera *et al.*, 2009) helping to maintain high biodiversity by selective infection of specific hosts. Hence increased lysis of a dominant strain leads to the establishment of a stable ecosystem efficiency as suggested by Rodriguez-Valera *et al.* (2009). Therefore, viral predators represent top-down control on prokaryotic communities (commonly used expression incorporating members of the domain *Bacteria* and *Archaea*; no phylogenetic relationship implied).

The killing-the-winner scenario also suggests that viruses enhance microbial community diversity (Suttle, 2007; Winter *et al.*, 2010). In this case 'winner' refers to the most successful taxon in terms of competition. Due to increased mortality rates generated by viral predation a higher species diversity can be sustained.

It is also widely assumed that due to infection, viruses can affect their hosts negatively but they can also have beneficial effects, for example, by augmenting metabolism, immunity, distribution, and evolution by implementing new genes (Rohwer & Thurber, 2009; Roossinck, 2011).

1.3 The microbial food web

Today we know that life in the ocean is microbe-based, putting autotrophic, heterotrophic and mixotrophic prokaryotes into the center (Barber & Hilting, 2000). They are not only primary producers by using light to fix carbon and generate oxygen, but also run carbon, oxygen, sulphur, and nitrogen cycles. An important pathway in the microbial food web is the microbial loop. This term was coined by Azam *et al.* (1983) and describes the release of dissolved organic carbon (DOC) into ambient water in different ways such as cell lysis, sloppy feeding caused by zooplankton, grazers, or the excretion by autotrophic picoplankton. Since most of the marine organisms are not able to utilize DOC directly it is of great importance that prokaryotes convert DOC into biomass and provide particulate organic carbon (POC) to higher trophic levels of the food web. In addition to flagellate grazing, bacterial cell lysis caused by viruses is a controlling factor in terms of efficiency of this cycle. Viruses are a major mechanism controlling microbial productivity since up to 70 % of the prokaryotes in the ocean are virally-infected at any given time (Wommack & Colwell, 2000). The effect of viral lysis of their host cells in addition to the release of progeny viruses is one of the main mechanisms releasing cellular compounds like sugars, peptides and other nutrients into ambient waters (Winter *et al.*, 2010). Thus, viruses are important drivers of marine geochemical cycles by implementing a shortcut of nutrients and carbon from organisms to the dissolved organic matter (DOM) pool. Therefore, this so-called *viral shunt* is effecting the rate of sinking POC (Weinbauer *et al.*, 2002) and may influence the biological pump by increasing community respiration and the conversion of DOC to POC which, in turn, might become available to higher trophic levels (Suttle, 2005). A low viral shunting efficiency leads to decreased bacterial growth efficiency (BGE) and less POC available for higher trophic levels (Motegi *et al.*, 2009).

1.4 Water masses in the North Atlantic

According to the definition of Tomczak (1999) "A water mass is a body of water with a common formation history, having its origin in a physical region of the ocean. Just as air-masses in the atmosphere, water masses are physical entities with measurable volume and therefore occupy a finite volume in the ocean."

In the course of this study, three different water masses were examined to address the question whether mixing of water masses exerts stimulating effects on prokaryotic and viral communities, viral production (VP), the frequency of infected cells (FIC), and the abundance of microorganisms.

The North Atlantic Deep Water (NADW) is characterized by a salinity of 34.9 to 35 and an average water temperature of 2° to 4°C. Its depth ranges from 1000 to 4000 m originating in the North Atlantic, mainly in the Labrador Sea and the Greenland-Iceland-Norwegian Sea. This oxygen-enriched water mass flows southwards (Tomczak & Godfrey, 2002). The Mediterranean Sea Overflow Water (MSOW) has its source in the Mediterranean Sea and extends from 1400 to 1600 m depth. The only connection to the Atlantic Ocean is the narrow and shallow Strait of Gibraltar, which is well known for its strong currents. The Mediterranean Sea is enclosed by the Eurasian and African continent and due to this isolation, the MSOW has a high temperature of up to 13°C. High salinity above 37 is a result of basin-scale turnover in winter leading to a uniform water column in the Mediterranean Sea. Due to the high eddy activity on the eastside of basins, the MSOW enters the NADW in the form of subsurface eddies (Tomczak & Godfrey, 2002).

The Antarctic Intermediate Water (AAIW) is defined by a temperature of 2.2°C and a comparatively low salinity of 33.8 ranging between a depth of 500 to 1000 m. AAIW has its origin in the Southern Ocean, moves northwards and enters the Atlantic Ocean at the coast of South America through the Drake Passage. The high amount of melting water off the Antarctic continent in the summer results in decreased salinity of the AAIW due to mixing with surface waters (Sverdrup *et al.*, 1942). During its flow to the north, AAIW is confined by other water masses and as it is entering the Subtropical Convergence, temperature and salinity increase to 3°C and 34.3, respectively (Tomczak & Godfrey, 2002).

2. MATERIAL AND METHODS

2.1 Experimental set-up and sampling

All samples used in this thesis were taken by Simone Muck, Nicole Köstner, and Christian Winter during the MEDEA-1 cruise on board R/V *Pelagia* in October 2011 at two stations (Station 2: N 40° E 13°; Station 7: N 42° E 20°) in the North Atlantic (Figure 2). In order to investigate the mixing effect of two different water masses, the following experiments were conducted: *Experiment 1* consisted of MSOW and NADW. The water masses of *Experiment 2* were AAIW and NADW. Of each water mass, 160 L were sampled and prokaryotic and viral concentrates were obtained by filtration. In addition, *in-situ* samples of every water mass were taken and stored for further analysis and comparison. The depth of the *in-situ* water sample of MSOW was 900 m, the one for AAIW was obtained at a depth of 1300 m and the depth of NADW was 2750 m at both stations. To concentrate prokaryotes, a Vivaflow 200 ultrafiltration device with a pore-size of 0.22 μm (Vivasciences) and Pelicon filter cassettes (PTGVPPC05) with a pore-size of 0.22 μm were applied. To obtain viral concentrates, spiral-wound ultrafiltration cartridges (Amicon S10Y100) with a 100 kDa molecular weight cut-off were used. For both experiments, the water masses as well as different prokaryotic communities were mixed together in duplicates leading to seven treatments and incubated in

20 L carboys for up to 72 h at *in-situ* temperature. The code used to abbreviate the treatments was generated like this: the prokaryotic concentrate of MSOW that was incubated in MSOW was abbreviated MSOW$_{prok}$/MSOW and e.g. prokaryotes from NADW incubated in AAIW are denoted as NADW$_{prok}$/AAIW.

2.2 Viral dilution approach

To obtain estimates of VP, the virus dilution approach was used. For best results, VP should be measured as directly as possible (Wilhelm *et al.*, 2002). Therefore, virus-free seawater was added to decrease the abundance of free-living viruses that could infect prokaryotic cells. Thus, VP represents the increase of viruses in the originally virus-free water over time. These viruses appearing during the incubation must have derived from previously infected cells. According to Winter *et al.* (2004) the following equation was applied:

$$VP = [(V_{max\,1} - V_{min\,1}) + (V_{max\,2} - V_{min\,2})]/(t_{max\,2} - t_{min\,1})$$

VP is given as viruses x 10^3 mL^{-1} h^{-1}, whereas V$_{max}$ and V$_{min}$ are highest and lowest measured viral abundances, respectively, during the incubation time.

This technique also allows to compute the frequency of infected cells (FIC) in % with the following equation as described by Winter *et al.* (2004):

$$FIC = \{[(V_{max} - V_{min})/burst\,size]/B_0\} \times 100$$

The BS was assumed to be 30 (Parada *et al.*, 20006) and B$_0$ represents the prokaryotic abundance at the beginning of the incubation.

FIC and VP were assessed during incubations over 32 h. The values given for 72 h are used as an additional discriminating factor to distinguish among treatment effects as re-infection might have occurred after prolonged incubation times.

2.3 Prokaryotic and viral abundance

Subsamples were taken in duplicate from the two experiments every 4 h for a total of 70 and 72 h. To determine prokaryotic and viral abundance, 1.8 mL of each sample were fixed with 36 µL of 25 % glutaraldehyde (final concentration of 0.5 %) for 10 min, followed by flash-freezing in liquid nitrogen and stored at -80°C until further analysis.

Counting of prokaryotes and viruses was performed with a FACS-AriaII flow cytometer (Becton Dickinson, San Jose, Calif.) and the corresponding software (BD FACSDiva v.6.1.3). Each sample was thawed in lukewarm water and subsequently diluted 1:2 to a final volume of 500 µL with TE buffer consisting of 10 mM Tris [Tris(hydroxymethyl)-aminomethan], 1 mM EDTA [ethylenediaminetetraacetic acid], pH 8.0 (Brussaard, 2004). The TE buffer has been filtered through an Acrodisc filter (0.2 µm) with a 50 mL syringe to ensure high quality measurements. All diluted samples were stained with 5 µL SYBRGreen I ([Invitrogen] diluted 1:200 of a 10.000 x stock solution) and incubated in the dark for 10 min. The samples for prokaryotic enumeration were incubated at room temperature (RT), samples for viral abundance were incubated at 80°C. To eliminate background noise, blanks were measured first, containing TE buffer and SYBRGreen I only. For every measurement, the flow rate was measured beforehand by using Milli-Q water at three different flow modes for 10 min each. The calculations of the three rates were based on weight before and after measuring. These values were converted to flow rates (µL min^{-1}) and integrated into a linear regression.

Prokaryotic abundance was determined using the following settings: Forward scatter (FSC) 470, side scatter (SSC) 500 and SYBRGreen I 500. For viral abundance, different settings were used: FSC 470, SSC 500 and SYBRGreen I 570. The threshold was set to 200 in the SYBRGreen I channel for both.

Prokaryotic cells and viruses were gated on cytograms of SSC versus SYBRGreen I fluorescence. According to the fluorescence intensity there were two distinguishable populations for prokaryotes: high nucleic acid cells (HNA) and low nucleic acid cells (LNA).

Viruses with high fluorescence intensity are referred to as VirHigh, with middle fluorescence as VirMed and with low fluorescence intensity as VirLow.

All calculations for prokaryotic and viral abundance were carried out with Microsoft Excel by using the measured events ($n_{measured}$), the number of blank events (n_{blank}), the used flow rate (FR) and the acquisition time (t_{acq}) given in min as well as the dilution factor (DF), the total volume (V_{total}) and the volume of the sample (V_{sample}) that has been used. To express the results in 10^5 cells/viruses mL^{-1} counts were divided by 100000.The data are given as the average of duplicate measurements.

The equation derived from these factors is as follows:

$$abundance \; = \left(\frac{n_{measured} - n_{blank}}{FR \times t_{acq}} \times DF \times \frac{V_{total}}{V_{sample}} \right) / 100000$$

2.4 Fingerprinting techniques

To obtain the community composition of prokaryotic and viral communities, two PCR-based fingerprinting methods were applied.

The method applied for viruses was randomly amplified polymorphic DNA polymerase chain reaction (RAPD-PCR). The advantage of this technique is that no previous sequence information is needed to obtain fingerprints of viral communities present in an environmental sample.

The second method used to obtain prokaryotic fingerprints was terminal restriction fragment length polymorphism (T-RFLP). Equally sized DNA fragments are separated according to differences in primary sequence upon digestion with a restriction enzyme (Marsh, 1999).

2.5 Prokaryotic community composition

Every 24 h, 2 L subsamples were filtered through a Millipore GVWP membrane filter (0.2 µm pore-size, 47 mm diameter), subsequently flash-frozen in liquid nitrogen and stored at -80°C.

Prokaryotic DNA was extracted using an UltraClean Soil DNA Isolation Kit (MoBio Cat. No.: 12800-100) following the manufacturer's manual. The DNA extracts were stored at -80°C until further treatment.

Gel electrophoresis of the DNA extracts was performed as quality check (75 V for 50 min) on a 1% agarose gel (Biozym LE Agarose Art. No.: 840004) using a SmartLadder (Eurogentec Cat. No.: MW-1700-10) as size marker and 1 x TBE buffer (1.34 M Tris, 0.44 M boric acid and 0.025 M EDTA, pH 8.4). All gels were stained with SYBR Gold (Invitrogen) in 1 x TBE buffer (10.000 x) for 30 min.

Amplification of 16S rRNA genes was done via PCR on a Master Cycler Pro (Eppendorf, Hamburg, Germany). The following primer pairs were used for *Bacteria*:

27 F-FAM (5' – AGA GTT TGA TCC TGG CTC AG – 3') and 1492 R-VIC (5' – GGT TAC CTT GTT ACG ACT T – 3'). The primer pairs used for *Archaea* were: 21 F-FAM (5' – TTC CGG TTG ATC CYG CCG GA – 3') and 958 R-VIC (5' YCC GGC GTT GAM TCC AAT T – 3'). The forward primers 27 F and 21 F were labeled with phosphoramidite fluorochrome 5-carboxyflourescin (FAM) at the 5'-end. Both reverse primers were VIC labeled at the 5'-end. Every PCR reaction contained 33.5 µL UV-treated Sigma-water, 5 µL of 10 x Taq buffer with KCl and $MgCl_2$, 4 µL of $MgCl_2$ (25 mM), 1.25 µL of dNTP (10 mM each [Invitrogen Cat. No.: 10297-018]), 2.5 µL of forward and reverse primer (10 µM each), 0.25 µL of Taq polymerase (5 U $µL^{-1}$ [Thermo Scientific Cat. No.: EP0621]) and 1 µL of prokaryotic DNA as template. The following PCR program was applied for the entire set of samples: one cycle at 95°C for 5 min for denaturation, 30 cycles at 95°C for 1 min, annealing at 55°C, elongation at 72°C, and finally one cycle at 72°C for 30 min. Negative controls without template DNA

were added to each PCR reaction. The PCR products were also checked on a 1% agarose gel (70 V for 50 min) and subsequently, purified with a 5Prime PCR Extract Mini Kit (Ref. No.: 2300610) following the manufacturer's instructions. The concentration of the purified PCR fragments was measured with a NanoDrop spectrophotometer and the associated software (v.1.1.9 by Thermo Scientific). The PCR products were stored at -20°C until further analysis. Digestion of the PCR products was done with the restriction enzyme *Hha*I (New England BioLabs R0139S). Every reaction contained 2.85 µL of Sigma water, 1.5 µL of 10 x NEB buffer 4, 0.15 µL of 100 x BSA, 0.5 µL *Hha*I (10 U µL^{-1}) and 10 µL of PCR fragments. The applied PCR program was run at 37°C for 12 h followed by 65°C for 20 min to ensure the inactivation of the restriction enzyme. The digested PCR products were stored at -20°C.

Digested PCR products (1 µL) were mixed with 490 µL of HiDi formamide and 9.9 µL 1200 LIZ size standard (Applied Biosystems Part No.: 4379450), denatured at 95°C for 3 min and put on ice immediately thereafter. Data were obtained on an automated capillary sequencer (Applied Biosystems 3130XL) and analyzed with the software Peak Scanner 1.0 (Applied Biosystems) applying the following peak minimum heights: 25 for blue corresponding to the FAM labeled forward primer, 25 for green corresponding to the VIC labeled reverse primer, and 20 for orange corresponding to the LIZ size standard. Microsoft Access and Excel presence/absence matrices were created for statistical analysis.

2.6 Viral community composition

Pre-filtered subsamples containing viruses but no prokaryotes (see above) were concentrated with a Vivaflow 200 ultrafiltration system with a molecular weight cut-off of 100 kDa to final volumes of 50 mL, immediately flash-frozen and stored at -80°C. Viral concentrates were thawed at room temperature and filtered through 0.2 µm Acrodisc filters into 50 mL tubes. The concentrates were centrifuged with Amicon Ultra Centrifugal filtering tubes (molecular weight cut-off: 100 kDa; Cat. No.: UFC 910096) to a final volume of 200 µL following the

manufacturer's instructions. For purification of viral DNA, a QIAamp MinElute Virus Spin Kit (Qiagen, Cat. No.: 57704) was used according to the handbook of the manufacturer. Amplification of viral DNA was performed using RAPD-PCR. The PCR mixture contained the following components: 36.25 µL Sigma water, 5 µL of 10 x Taq buffer with KCl, 1.5 µL MgCl$_2$ (50 mM), 1 µL of dNTP (10 mM each), 5 µL of the decamer primer CRA-22 (5' – CCG CAG CCA A – 3') or 10 µL of OPA-13 (5' – CAG CAC CCA C – 3'), 0.25 µL of Platinum Taq DNA Polymerase (Invitrogen, Cat. No.: 10966-026) and 1 µL of viral DNA as template. In each reaction, only one primer was used, acting as both the forward and the reverse primer. Negative controls without template DNA were performed for each run. The PCR program was as follows: 94°C for 10 min, 30 cycles at 94°C for 30 s, 35°C for 3 min, and 72°C for 1 min, and finally 72°C for 30 min. All RAPD-PCR products were separated by gel electrophoresis on 2.5% agarose gels run in TBE buffer (44 V for 135 min) and visualized by SYBRGold staining and a Gel Doc EQ digital gel imaging system (BioRad). The gels were analyzed with the software Quantity One (v. 4.6.8) using the size standards SmartLadder and Fermentas gene ruler (Cat. No.: SM0311). The bands were sized according to these two size standards. To ensure precise basepair numbers, a background subtraction was performed for each gel. Based on the resulting patterns, a presence/absence matrix was created with Microsoft Excel.

2.7 Statistical analysis

Based on the results of T-RFLP and RAPD-PCR, presence/absence matrices were created to compare the prokaryotic and viral community dynamics. The software PAST (v. 2.16 created by Hammer & Harper 2009) allowed to perform Mantel tests by calculating Jaccard distance matrices. This analysis was applied for the two experiments comparing the community composition of prokaryotes and viruses. Mantel tests are the matrix equivalent of a correlation coefficient commonly applied to scalar data. Mantel tests (r_M) were considered to be relevant

at $r_M > 0.5$. The software PAST was also used to perform cluster analysis based on Jaccard distance for compositional data obtained by T-RFLP and RAPD-PCR.

3. RESULTS

3.1 Prokaryotic and viral abundance

The average *in-situ* prokaryotic abundance was 0.67×10^5 mL^{-1} for Station 2/900 m (MSOW) and 0.26×10^5 mL^{-1} for Station 2/2750 m from NADW (Table 1). Viral abundance for Station 2/900 m was 15.45×10^5 mL^{-1} and 7.57×10^5 mL^{-1} for Station 2/2750 m. In *Experiment 2* prokaryotic abundance was 0.44 and 0.22×10^5 mL^{-1} for Station 7/1300 m and Station 7/2750 m, respectively. By plotting prokaryotic and viral abundance over the incubation time it became visible that there was no drastic change in prokaryotic abundances in all seven treatments and in both experiments. In *Experiment 1* viral abundance was on average one order of magnitude higher than prokaryotic abundance (Figure 3) although viral abundances varied from 0.38 to 6.2×10^5 mL^{-1}. Prokaryotic abundance ranged from 0.05 to

0.38×10^5 mL^{-1}. There was an increase of viruses in all treatments in *Experiment 1*. The highest values of viral abundance were found in *Experiment 1* NADW$_{prok}$/MSOW with 5.6×10^5 mL^{-1} after 52 h of incubation (Figure 3c), whereas prokaryotic abundance with 0.08×10^5 mL^{-1} showed the lowest values in *Experiment 1* and a virus-to-prokaryote ratio (V/P) of 32.5. The lowest V/P ratio was measured in MSOW$_{prok}$/NADW. Viral abundance was 16 times higher than prokaryotic abundance in *Experiment 1* (Table 1). Prokaryotic abundance was between 1.3 and 2 times lower in *Experiment 2* compared to *Experiment 1*. The V/P ratio in *Experiment 2* varied between 2.1 and 7.4. The highest V/P ratio with 12.9 was found in NADW$_{prok}$/AAIW (Table 2).

3.2 Prokaryotic and viral populations

In *Experiment 1*, the dominant population was the HNA fraction with an average of 56.8 %. The highest value was detected in $NADW_{prok}/MSOW$ with 61.8 %, whereas the LNA fraction reached 38.2 % of total prokaryotic abundance. The lowest relative abundance of the HNA population was 53.4 % in $MSOW_{prok}/MSOW$ (Table 3). The predominant viral population was the VirLow group with 71.7 % in *Experiment 1*, followed by the VirMed fraction with 27.8 % and VirHigh cells with 0.5 %. The highest percentage of VirLow cells was reached in $NADW_{prok}/NADW$ with 74.7 %, whereas the least abundant population was VirMed (24.8 %). The VirHigh population constituted 0.5 % in the same treatment $NADW_{prok}/NADW$ (Table 3). VirLow was least abundant in $MSOW_{prok}NADW_{prok}/NADW$ with 68.8 %, whereas the VirMed fraction reached its highest value in this treatment in *Experiment 1* with 30.1 %.

The results of *Experiment 2* differed from the ones of *Experiment 1* concerning the population distribution of HNA and LNA cells (Table 4). HNA was still the dominant population of prokaryotic cells with 58.9 % on average. Highest HNA abundance was detected in $AAIW_{prok}/AAIW$ with 61.4 % and lowest in $NADW_{prok}/AAIW$ with 56.6 %. In comparison with *Experiment 1*, the distribution within viral populations shifted in *Experiment 2* towards VirHigh at the expense of VirMed. On average the predominant population was VirLow accounting for 82.3 %, followed by VirMed with 15.5 % and VirHigh with 2.2 % of total viral abundance. The highest contribution of VirLow was reached in $NADW_{prok}/AAIW$ with 88.9 %, in $NADW_{prok}/NADW$ for VirMed with 27.4 %, and for VirHigh with 6.2 %

(Table 4).

3.3 Frequency of infected cells

FIC during the two experiments showed pronounced variations within 32 and 72 h of incubation (Figures 5 and 6). Highest FIC throughout the dataset was detected in $NADW_{prok}/MSOW$ and $NADW_{prok}/AAIW$, respectively. FIC reached 221 % and 517 % after

32 h and 72 h, respectively, in *Experiment 1*. This is an inter-experimental trend since in *Experiment 2* highest FIC was also detected in $NADW_{prok}/AAIW$ with 97 % after 32 h and 206 % after 72 h of incubation.

Overlapping percentages of the different treatments allowed arranging them into groups of similar values when the ranges of the duplicates were also taken into account. The variation in FIC between duplicate incubations was used to distinguish distinct groups in the data (lower case letters in Figures 5 - 8) Within *Experiment 1* there were significant differences between $MSWO_{prok}/MSOW$, $MSOW_{prok}/NADW$, and $MSOW_{prok}NADW_{prok}/NADW$ forming group a and $NADW_{prok}/MSOW$, $NADW_{prok}/NADW$) and $MSOW_{prok}NADW_{prok}/MSWO/NADW$ forming group b after 32 h of incubation (Figure 5). FIC of $MSOW_{prok}NADW_{prok}/MSOW$ (group ab) overlapped with groups a and b.

After 72 h four groups were distinguishable (Figure 5). The treatments $MSOW_{prok}/MSOW$, $MSOW_{prok}/NADW$, $MSOW_{prok}NADW_{prok}/MSOW$, and $MSOW_{prok}NADW_{prok}/NADW$ were forming group a, whereas $NADW_{prok}/MSOW$ formed a single group b as well as $NADW_{prok}/NADW$ in group c. $MSOW_{prok}NADW_{prok}/MSOW/NADW$ showed attributes of group a and c.

The differences between the groups of FIC in *Experiment 2* were more pronounced and resulted in more groups (Figure 6).FIC in $AAIW_{prok}/AAIW$ formed a single group a after 32 h, as well as $AAIW_{prok}/NADW$ (group b) and $NADW_{prok}/AAIW$ (group c). $AAIW_{prok}NADW_{prok}/NADW$ and $AAIW_{prok}NADW_{prok}/AAIW/NADW$ formed group d, whereas $NADW_{prok}/NADW$ was not different from groups a and b (group ab) and $AAIW_{prok}NADW_{prok}/AAIW$ showed similarities to groups b and d (group bd). There were also four main groups of FIC after 72 h of incubation in *Experiment 2*. $AAIW_{prok}/AAIW$, $AAIW_{prok}/NADW$, and $AAIW_{prok}NADW_{prok}/NADW$ formed group a. $NADW_{prok}/AAIW$ established a single group b, as well as $NADW_{prok}/NADW$ (group c) and

AAIW$_{prok}$NADW$_{prok}$/AAIW/NADW (group d). There were no significant differences between groups a and d in AAIW$_{prok}$NADW$_{prok}$/AAIW (group ad).

3.4 Viral Production

Within 32 h, VP ranged from 0.13 to 0.23 x 10^3 mL^{-1} h^{-1} in *Experiment 1* (Figure 7). Highest VP was detected in NADW$_{prok}$/MSOW and lowest in MSOW$_{prok}$/ MSOW. After 72 h of incubation, VP varied between 0.14 and 0.19 x 10^3 mL^{-1} h^{-1} (Figure 7). Highest VP was also found in NADW$_{prok}$/MSOW and lowest in NADW$_{prok}$/NADW. After 32 h, two main groups of VP developed with MSOW$_{prok}$/MSOW, NADW$_{prok}$/NADW, and MSOW$_{prok}$NADW$_{prok}$/NADW as group a and MSOW$_{prok}$/NADW, NADW$_{prok}$/MSOW, and MSOW$_{prok}$NADW$_{prok}$/MSOW/NADW as group b. MSOW$_{prok}$NADW$_{prok}$/MSOW formed group ab. Three main groups were formed after 72 h of incubation, containing NADW$_{prok}$/MSOW as group a, NADW$_{prok}$/NADW as group b, and MSOW$_{prok}$NADW$_{prok}$/NADW as group c.

In *Experiment 2*, VP varied between 0.02 and 0.09 x 10^3 mL^{-1} h^{-1} (Figure 8) within the initial 32 h incubation, as well as over 72 h. The highest VP found in NADW$_{prok}$/AAIW was therefore 2.5 times lower than in *Experiment 1*. The highest ranges within the duplicates were detected in MSOW$_{prok}$NADW$_{prok}$/MSOW and AAIW$_{prok}$NADW$_{prok}$/AAIW in *Experiment 1* and *2*, respectively.

After 32 h three main groups were visible with group a of AAIW$_{prok}$/AAIW, AAIW$_{prok}$/NADW, AAIW$_{prok}$NADW$_{prok}$/AAIW, and AAIW$_{prok}$NADW$_{prok}$/NADW. NADW$_{prok}$/AAIW and formed another group.

3.5 Prokaryotic community composition

The size of bacterial DNA fragments ranged from 26 to 1111 basepairs (bp) for the forward primer with overall 35 distinct peaks in *Experiment 1* (Figure 11). The most common peaks were detected at 31, 33, and 903 bp. With 18 peaks in total, sample B1-T18 ($MSOW_{prok}$/MSOW after 70 h of incubation) contained the highest number of peaks, whereas samples B1-T6, A4-T6 and B5-T6 ($MSOW_{prok}$/NADW; $NADW_{prok}$/NADW and $MSOW_{prok}NADW_{prok}$/MSOW after 25 h of incubation) contained only 2 peaks. At *Station 2/900 m*, two peaks were detected at 29 and 903 bp and at *Station 2/2750 m* at 30 and 903 bp. These two samples are considered to be the T_0 samples for the experiments. Cluster analysis revealed two main groups (Figure 12a). It appeared that samples with the same incubation time clustered together and both T_0 samples fell into the same cluster.

Using the reverse primer for *Bacteria*, in total 46 distinct peaks were detected ranging from 28 to 527 bp (Figure 13). The most common peaks occurred at 33, 34, and 389 bp. The samples B1-T18 and B5-T12 ($MSOW_{prok}$/MSOW after 70 h of incubation and $MSOW_{prok}NADW_{prok}$/MSOW after 48 h of incubation) exhibited the highest number (20) of peaks. Both T_0 samples from *Station 2/900 m* and *Station 2/2750 m* were characterized by five peaks each differing in terms of distribution. By clustering the samples, three main groups appeared of which the first one was mainly composed of samples that belong to NADW prokaryotes (Figure 12b). *Station 2/2750 m* belonged also to this group. In the second cluster, MSOW was predominant and included the T_0 sample *Station 2/900 m*.

Archaeal DNA fragments with the forward primer ranged from 27 to 913 bp in *Experiment 1* (Figure 17) with a total of 9 peaks. The DNA fragment with 322 bp was present in 41 out of 42 samples. The reverse archaeal primer yielded a total number of 10 peaks. The fragment with 586 bp appeared in 40 out of 42 samples. *Station 2/900 m* showed four peaks at 322, 331, 585 and 913 bp. At *Station 2/2750 m* only two peaks at 322 and 331 bp were detected.

The archaeal reverse primer yielded six peaks at *Station 2/900 m* and three peaks at *Station 2/2750m* (Figure 19). Cluster analysis revealed three groups within data obtained from the archaeal forward primer (Figure 18a). Group A is a mixture of both water masses (MSOW and NADW), whereas the second group was mainly characterized by NADW and MSOW and *Station 2/2750 m*. The third cluster was composed of mainly T12 and T18 samples of both water masses and of *Station 2/900 m*. Cluster analysis of data obtained from the archaeal reverse primer revealed three main groups. MSOW prokaryotes were predominant in group A and NADW prokaroytes in group B (Figure 18b). The T_0 samples clustered together in the third group.

In *Experiment 2* the bacterial DNA fragments ranged from 22 to 1053 bp for the forward primer. Overall 32 distinct peaks were detected. The most common peaks were the fragments with 31, 33, and 903 bp. The sample B2-T18 ($AAIW_{prok}$/NADW; 70 h of incubation) showed most peaks (16). There were no peaks detected in sample B2-T6 ($AAIW_{prok}$/NADW after 24 h of incubation) and A3-T12 ($NADW_{prok}$/AAIW; 48 h of incubation). The T_0 samples *Station 7/1300 m* and *Station7/2750 m* showed little variation in peak distribution with six and four peaks, respectively (Figure 14). Cluster analyses of data obtained from the bacterial forward primer exhibited three main groups: the first was mainly composed of NADW, mainly $AAIW_{pork}NADW_{prok}$/NADW and $AAIW_{prok}NADW_{prok}$/AAIW/NADW. The second group was basically composed of the treatments $AAIW_{prok}$/AAIW and $AAIW_{prok}$/NADW
(Figure 15a).

The distribution of peaks for data obtained with the bacterial reverse primer ranged from 27 to 529 bp in *Experiment 2*, with a total number of 35 distinct peaks. The most common peaks were the fragments with 33, 39, and 134 bp. The sample with most peaks was B2-T18 (19) belonging to treatment $AAIW_{prok}$/NADW. There were no peaks detected in samples A3-T12 ($NADW_{prok}$/AAIW) and B7-T6 belonging to treatment $AAIW_{prok}NADW_{prok}$/AAIW/NADW

(Figure 16). The T_0 samples *Station 7/1300m* and *Station 7/2750 m* showed seven and four peaks, respectively, which were congruent with the most common peaks detected throughout the experiment.

Cluster analysis of data obtained with the bacterial reverse primer indicated two main groups (Figure 15b). The sample *Station 7/1300 m* belonged to the first cluster, which was characterized by the water mass NADW, mainly $AAIW_{prok}NADW_{prok}/NADW$ and $AAIW_{prok}NADW_{prok}/AAIW/NADW$. The second group contained *Station 7/2750 m* and was dominated by the water mass AAIW.

The archaeal DNA fragments in *Experiment 2* for the forward primer ranged from 27 to 913 bp with a total number of 10 peaks. The most common peak at 322 bp was found in 40 out of 42 samples. The sample with the highest number of peaks was A4-T6 ($NADW_{prok}/NADW$) with six peaks in total. Each T_0 sample *Station 7/1300 m* and *Station7/2750 m* showed three peaks, congruent with the most common peaks in the dataset (Figure 20). In the cluster analysis of data obtained with the archaeal forward primer, three groups were detected (Figure 21a). The T_0 sample *Station 7/1300 m* and *Station 7/2750 m* clustered together, the second cluster was characterized by water obtained with NADW and the third cluster consisted of the water mass AAIW samples.

The size of digested PCR fragments obtained from the archaeal forward primer varied from 29 to 914 bp with a total of 10 distinct peaks in *Experiment 2*. The samples with most peaks were A1-T18 and A2-T18 ($AAIW_{prok}/AAIW$ and $AAIW_{prok}/NADW$) with eight peaks after an incubation time of 72 (Figure 22). The most common peaks, were the fragments at 29, 363, and 586 bp. This was similar to the T_0 samples *Station 7/1300 m* and *Station 7/2750 m* with five and seven peaks, respectively. Two main clusters were identified using the cluster

analysis (Figure 21b). NADW dominated over AAIW in group A, whereas samples with longer incubation time (12 and 18 hours) dominated the second cluster also containing both T_0 samples.

3.6 Viral community composition

The size of viral RAPD-PCR fragments ranged from 185 to 3715 bp for the primer CRA-22 in *Experiment 1* and comprised 48 distinct bands. The two most common bands had a size of 349 and 791 bp occurring in 95 % of the samples from *Experiment 1* (Figure 23). With a total number of 20 bands, the sample A1-T6 ($MSOW_{prok}$/MSOW) contained more than twice as much as the average number of bands (9) per sample throughout *Experiment 1*. The T_0 samples *Station 2/900 m* and *Station 2/ 2750 m* comprised 14 and 18 bands in total, respectively. Cluster analysis revealed four main groups. In group A, T_0 samples clustered together with the treatment $MSOW_{prok}NADW_{prok}$/NADW (Figure 24a). The second group was dominated by the water mass MSOW and $MSOW_{prok}$/NADW. In group C mainly $MSOW_{prok}$/MSOW and $NADW_{prok}$/MSOW were found. The water obtained with NADW prevailed in the group D where $NADW_{prok}$/NADW and $MSOW_{prok}NADW_{prok}$/MSOW/NADW dominated due to mixing of both waters and prokaryotes.

With the viral primer OPA-13, 31 distinct bands were detected in *Experiment 1* with RAPD-PCR fragments ranging in size from 352 to 3473 bp. Sample A4-T18 ($NADW_{prok}$/NADW) exhibited the highest number of bands (14 bands), whereas the average number of bands per sample was eight (Figure 26). The most common bands in *Experiment 1* were the bands with 412, 680, 957, 1216, 1616, and 2092 bp in size. Together, they comprised between 48 and 62 % of all detected bands in *Experiment 1*. The two samples from the starting point of the incubation (*Station 2*) accounted for 10 and 8 bands, however, the banding pattern varied substantially compared with all treatments within *Experiment 1*. Taking all treatments of

Experiment 1 together, cluster analysis revealed two main groups, the first one dominated by MSOW prokaryotesand the second one by NADW water including the T_0 samples (Figure 27a).

In *Experiment 2*, viral RAPD-PCR fragments varied from 185 to 3715 bp for primer CRA-22. In total, 47 distinct bands were detected with an average of six bands per sample. The most common bands were the fragments with 340 and 791 bp in size, which were found in 95 % of all the samples.

The sample with most bands was B7-T6 ($AAIW_{prok}NADW_{prok}$/AAIW/NADW) with 17 bands. At *Station 7/1300 m* and *Station 7/2750 m* 15 and 13 bands, respectively, were detected. (Figure 25) Cluster analyses revealed four groups. Group A was dominated by $AAIW_{prok}NADW_{prok}$/NADW and *Station 7/2750 m* and therefore, mostly comprised of NADW prokaryotes. The second group was also dominated by prokaryotes from NADW and *Station 7/1300 m*. Group C was mainly comprised of AAIW prokaryotes, whereas group D was a mixture of both AAIW and NADW prokaryotes (Figure 24b).

In total, 33 distinct viral bands were detected with the primer OPA-13 in *Experiment 2*. The most common bands were the fragments with 660, 1240, and 1601 bp. The sample with most bands was B2-T6 ($AAIW_{prok}$/NADW) with 19 bands. The T_0 samples *Station7/1300 m* and *Station 7/2750 m* showed almost the same number of bands with 15 and 14 bands, respectively, and were nearly congruent (Figure 28). Cluster analysis revealed six groups (Figure 27b). Group A comprised $NADW_{prok}$/NADW and NADW, and the second group consisted mainly of AAIW prokaryotes. The T_0 samples clustered together with $AAIW_{prok}NADW_{prok}$/AAIW.

3.7 Correlation of prokaryotic and viral communities

Mantel tests revealed that the bacterial peak pattern with the forward and reverse primer was related to each other (Table 5). However, there were no correlations between the forward and reverse primer for *Archaea* or for data obtained by the two viral primers. Data obtained from the duplicate incubations by the bacterial forward primer were positively correlated in *Experiment 1* for $MSOW_{prok}/MSOW$ and $MSOW_{prok}NADW_{prok}/NADW$ only. In *Experiment 2*, only $AAIW_{prok}NADW_{prok}/AAIW/NADW$ showed a positive correlation between the duplicates of the bacterial forward primer (Table 6). Strong correlations were found in *Experiment 1* for the bacterial reverse primer in $MSOW_{prok}/NADW$ as well as in *Experiment 2* for $NADW_{prok}/NADW$ and $AAIW_{prok}NADW_{prok}/NADW$. There were only three correlations between duplicates for the archaeal forward primer of both experiments. Most of the duplicates of the archaeal reverse primer were correlated in both experiments.

Data from the viral primer CRA-22 comprised one positive correlation between duplicates in $MSOW_{prok}/MSOW$ in *Experiment 1*, whereas viral banding patterns obtained from primer OPA-13 were correlated in almost all duplicates in both experiments.

A relation between duplicates and between the two experiments was found in $NADW_{prok}/NADW$ for data from the bacterial forward primer and in the treatments $MSOW_{prok}/MSOW$ and $AAIW_{prok}/AAIW$, respectively, and in $MSOW_{prok}NADW_{prok}/MSOW$ for data from the bacterial reverse primer. There were no correlations found for data from the archaeal primers and primer CRA-22. Duplicates banding patterns obtained by the primer OPA-13 were correlated in $MSOW_{prok}NADW_{prok}/NADW$ and the treatment $MSOW_{prok}NADW_{prok}/MSOW/NADW$ and $AAIW_{prok}NADW_{prok}/AAIW/NADW$, respectively (Table 7).

4. DISCUSSION

4.1 Prokaryotic and viral abundance

The use of flow cytometry allowed comparing prokaryotic and viral abundance of the *in-situ* samples to previous studies conducted in adjacent areas in the Atlantic Ocean, which found similar abundances using the same method (Parada *et al.*, 2007; De Corte *et al.*, 2010). Viral and prokaryotic abundance decreased and V/P ratios of both T_0 samples increased with depth as previously reported (Weinbauer & Rassoulzadegan, 2004; Winter *et al.*, 2008). While Winter *et al.* (2004) detected one or two peaks in viral abundance during the course of incubations using the virus dilution approach, 2-4 peaks were detected in this study. Winter *et al.* (2004) rejected the possibility that new infection could be causing these abundance peaks but instead suggested that the appearance of two peaks is due to different viral populations with different latent periods. We can also rule out new infection as the cause of the multiple viral abundance peaks during the incubations, since the viral latent period should be related to prokaryotic generation time (Proctor *et al.*, 1993; Binder, 1999), which is much longer in oceanic waters (Fuhrman *et al.* 1989). In both experiments, prokaryotic abundance remained fairly stable during the incubation in all treatments and experiments.

In our incubations the highest V/P ratio was found when prokaryotic concentrates of NADW were mixed with MSOW and AAIW (Table 1 and 2). A possible explanation for this trend could be a higher rate of previously infected cells in the NADW where the lysogenic life cycle might dominate over the lytic pathway. Overall there were lower prokaryotic and viral abundances detected in the samples of *Experiment 2*, which were obtained at Station 7. This sampling station was located more offshore then Station 2. According to Weinbauer (2004) viral abundance will decrease from coastal to offshore waters and could explain these findings.

4.2 Frequency of infected cells and viral production

The BS can obtained by counting viruses in visibly infected prokaryotes using transmission electron microscopy. In this study, a BS of 30 was assumed for all water masses and experiments based on previous studies from a variety of aquatic environments (Wommack & Colwell, 2000; Weinbauer *et al.*, 2003; Parada *et al.*, 2006). The applied BS of 30 might have been too low, since FIC repeatedly reached values above 100 %. The treatments MSOW$_{prok}$/MSOW, AAIW$_{prok}$/AAIW, NADW$_{prok}$/NADW represented the negative controls In *Experiment 1*, FIC in the treatments MSOW$_{prok}$/MSOW and NADW$_{prok}$/NADW was 61 % and 128 % within 32 h of incubation (Figure 5).

Unrealistically high FIC values were also found in *Experiment 2*, except in NADW$_{prok}$/NADW (Figure 6). FIC in the negative controls of *Experiment 2* (AAIW$_{prok}$/AAIW and NADW$_{prok}$/NADW) were much lower and remained below 100 %.

Overall, trends in FIC after 32 and 72 h of incubation were similar for both experiments (Figures 5 and 6). The comparison of the negative control MSOW$_{prok}$/MSOW with MSOW$_{prok}$/NADW did not reveal significant changes in FIC over 32 and 72 h in *Experiment 1*. However, FIC in NADW$_{prok}$/MSOW was significantly higher compared to the negative control NADW$_{prok}$/NADW over 32 h and this difference was even more pronounced after 72 h. The same pattern was found in *Experiment 2*. This treatment effect was much smaller in MSOW$_{prok}$NADW$_{prok}$/MSOW/NADW and not detectable in MSOW$_{prok}$NADW$_{prok}$/MSOW and MSOW$_{prok}$NADW$_{prok}$/NADW. In *Experiment 2* AAIW$_{prok}$NADW$_{prok}$/NADW and AAIW$_{prok}$NADW$_{prok}$/AAIW/NADW showed a significantly higher FIC then both negative controls but FIC in NADW$_{prok}$/AAIW was still highest after 32 h and 72 h of incubation.

When VP rates were compared, similar patterns as for FIC were found (Figures 7 and 8).

In *Experiment 1* VP in both negative controls was similar to each other during during the entire incubation period and again NADW$_{prok}$/MSOW exhibited the highest increase in VP after 32 and 72 h. In both experiments the treatments MSOW$_{prok}$NADW$_{prok}$/MSOW/NADW and AAIW$_{prok}$NADW$_{prok}$/AAIW/NADW showed also increased VP rates but remained below VP of NADW$_{prok}$ in either MSOW or AAIW water. A higher density of host cells due to the mixing of two prokaryotic concentrates might be a possible explanation for these increased values.

In *Experiment 2*, the negative control NADW$_{prok}$/NADW exhibited the lowest VP after 32 and 72 h. The other negative control, AAIW$_{prok}$/AAIW was similar to the mixing treatments (Figure 8). Again the NADW$_{prok}$/AAIW showed the highest VP over 32 and 72 h.

Overall in both experiments FIC and VP increased significantly when prokaryotes of NADW were mixed with MSOW or AAIW, whereas these effects were much lower or not detectable for MSOW and AAIW.

4.3 Prokaryotic and viral community composition within experimental treatments

The fingerprinting techniques used in this study to investigate bacterial, archaeal, and viral community composition were applied in previous studies and are assumed to detect mostly abundant OTUs (Moeseneder et al., 1999; Winter & Weinbauer, 2010).

The number of distinct bacterial peaks of the *in-situ* samples varied between the two experiments. The number of OTUs of the T_0 samples in the archaeal and viral community was similar to those of De Corte *et al.* (2010). However, the incubation experiments revealed no clear trend within treatments in terms of number of peaks or bands, which remained rather constant during the course of the incubation. Mantel tests were used to quantify the relationship between duplicates of the treatments, as well as between the experiments. The Mantel statistics calculated between the duplicate incubations for data obtained by the

forward and the reverse primer for *Bacteria* were variable over both experiments (Table 6). Due to the relatively low number of distinct peaks detected for *Archaea* even rather small changes in the number of peaks in a given sample might have a strong impact on the outcome of the Mantel analysis. In the bacterial community 4- to 5-fold more peaks were detected than in *Archaea*. Only small treatment effects in the bacterial community composition were detected because bacterial communities in most treatments did not correspond between duplicate incubations indicating the prevalence of stochastic effects. In contrast the Mantel statistics calculated between the duplicate incubations for data obtained by the archaeal reverse primer revealed that for most treatments archaeal communities between the duplictaes corresponded well with each other indicating a prevalence of treatment effects over stochastic effects.

The two viral primers used in this study have been shown to detect two different subsets of the viral community (Winter & Weinbauer 2010). Viral community composition as determined by the primer CRA-22 was hardly ever correlated between the duplicate incubations of the treatments. In contrast, data obtained by the primer OPA-13 was correlated between the duplicate incubations for most of the treatments over the entire incubation period suggesting a strong treatment effect on this group of viruses.

4.4 Summary and conclusion

In-situ samples of prokaryotic and viral abundance agreed well with previous findings. Also, the number of bands and peaks detected for bacterial, archaeal, and viral communities by the used methods is similar to previous studies. The two incubation experiments revealed inter-experimental trends for FIC and VP. Incubating prokaryotes originating from NADW in either MSOW or AAIW resulted in significantly higher FIC and VP as compared to the negative controls. A possible explanation for this is the predominance of lysogenic viruses in NADW prokaryotes, which upon mixing with other water masses are entering the lytic cycle.

Other treatments with two prokaryotic concentrates transferred into other water masses showed also increased values in FIC and VP relative to the water masses to which indigenous prokaryotic communities were added but these values were not significantly higher than the negative controls. Mantel tests revealed that the community detected with the archaeal reverse primer seemed to be driven mainly by treatment effects as well as the viral community detected with the primer OPA-13.

In conclusion, the research question addressed in this thesis whether mixing of water masses exerts stimulating effects on prokaryotic and viral communities can be positively answered since both, FIC and VP, increased in the treatments where prokaryotes originating from NADW were incubated in water from MSOW and AAIW.

ACKNOWLEDGEMENTS

5. LITERATURE

Ackermann HW.(2003). Bacteriophage observations and evolution. *Res Microbiol* 154: 245-251.

Azam F, Fenchel T, Field JG, Gray JS, Meyer-Reil LA, Thingstad F (1983). The ecological role of water-column microbes in the sea. *Mar Ecol-Prog Ser* 10: 257-263.

Barber RT, Hilting AK (2000). Achievements in biological oceanography. In: 50 Years of Ocean Discovery. National Academy Press, Washington DC.

Binder BJ (1999). Reconsidering the relationship between virally induced bacterial mortality and frequency of infected cells. *Aquat Microb Ecol* 18: 207-215

Brussaard CPD, Marie D, Bratbak G (2000). Flow cytometric detection of viruses. *J Virol Methods* 85: 175-182.

Brussaard CPD (2004). Optimization of Procedures for Counting Viruses by Flow Cytometry. *Appl Environ Microb* 70: 1506-1513.

De Corte D, Sintes E, Winter C, Yokokawa T, Reinthaler T, Herndl GJ (2010). Links between viral and prokaryotic communities throughout the water column in the (sub)tropical Atlantic Ocean. *ISME J* 4: 1431-1442.

Edwards RA, Rohwer F (2005). Viral metagenomics. *Nat Rev Micro* 3: 504-510.

Fuhrman JA, Sleeter TD, Carlson CA, Proctor LM (1989). Dominance of bacterial biomass in the Sargasso Sea and its ecological implications. *Mar Ecol-Prog Ser* 57: 207-217

Hendrix RW, Smith MC, Burns RN, Ford ME, Hatfull GF (1999). Evolutionary relationships among diverse bacteriophages and prophages: all the world's a phage. *P Natl Acad Sci USA* 96: 2192-2197.

Marsh TL (1999). Terminal restriction fragment length polymorphism (T-RFLP): An emerging method for characterizing diversity among homologous populations of amplification products. *Curr Opin Microbiol* 2: 323-327.

Moeseneder MM, Arrieta JM, Muyzer G, Winter C, Herndl GJ (1999). Optimization of terminal-restriction fragment length polymorphism analysis for complex marine bacterioplankton communities and comparison with denaturing gradient gel electrophoresis. *Appl Environ Microb* 65(8): 3518-3525.

Motegi C, Nagata T, Miki T, Weinbauer M, Legendre L, Rassoulzadegan F (2009). Viral control of bacterial growth efficiency in marine pelagic environments. *Limnol Oceanogr* 54: 1901-1910.

Munn CB (2006). Viruses as pathogens of marine organisms - from bacteria to whales. *J Mar Biol Assoc UK* 86: 453-467.

Parada V, Herndl GJ, Weinbauer MG (2006). Viral burst size of heterotrophic prokaryotes in aquatic systems. *J of the Mar Biol Assoc UK* 86: 613-621.

Parada V, Sintes E, van Aken HM, Weinbauer MG, Herndl GJ (2007). Viral Abundance, Decay, and Diversity in the Meso- and Bathypelagic Waters of the North Atlantic. *Appl Environ Microb* 73: 4429-4438.

Proctor LM, Okubo A, Fuhrman JA (1993). Valibrating estimates of phage-induced mortality in marine bacteria: ultrastrucural studies of marine bacteriophage development from one-step growth experiments. *Microb Ecol 25*: 161-182

Reinthaler T, van Aken H, Veth C (2006). Prokaryotic Respiration and Production in the Meso- and Bathypelagic Realm of the Eastern and Western North Atlantic Basin. *Limnol Oceanogr* 51: 1262-1273.

Rodriguez-Valera F, Martin-Cuadrado A-B, Rodriguez-Brito B, Pasic L, Thingstad TF, Rohwer F, Mira A (2009). Explaining microbial population genomics through phage predation. *Nat Rev Micro* 7: 828-836.

Rohwer F, Thurber RV (2009). Viruses manipulate the marine environment. *Nature* 459: 207-212.

Roossinck MJ (2011). The good viruses: viral mutualistic symbioses. *Nat Rev Micro* 9: 99-108.

Suttle CA (2005). Viruses in the sea. *Nature* 437: 356-361.

Suttle CA (2007). Marine viruses - major players in the global ecosystem. *Nat Rev Micro* 5: 801-812.

Sverdrup HU, Johnson MW, Fleming RH (1942). The Oceans, Their Physics, Chemistry, and General Biology. Prentice-Hall, New York.

Tomczak M (1999). Some historical, theoretical and applied aspects of quantitative water mass analysis. *J Mar Res* 57: 275-303.

Tomczak M, Godfrey JS (2002). Regional Oceanography: An Introduction. Daya Publishing House, Delhi.

Weinbauer MG, Winter C, Höfle MG (2002). Reconsidering transmission electron microscopy based estimates of viral infection of bacterio- plankton using conversion factors derived from natural communities. *Aquat Microb Ecol* 27: 103-110.

Weinbauer MG, Brettar I, Höfle MG (2003). Lysogeny and Virus-Induced Mortality of Bacterioplankton in Surface, Deep, and Anoxic Marine Waters. *Limnol Oceanogr* 48: 1457-1465.

Weinbauer MG (2004). Ecology of prokaryotic viruses. *FEMS Microbiol Rev* 28: 127-181.

Weinbauer MG & Rassoulzadegan F (2004). Are viruses driving microbial diversification and diversity? *Environ Microbiol* 6: 1-11.

Wilhelm SW, Brigden SM, Suttle CA (2002). A Dilution Technique For The Direct Measurement Of Viral Production: A Comparison In Stratified And Tidally Mixed Coastal Waters. *Microb Ecol* 43: 168-173.

Winget DM, Wommack KE (2008). Randomly Amplified Polymorphic DNA PCR as a Tool for Assessment of Marine Viral Richness. *Appl Environ Microb* 74: 2612-2618.

Winter C, Herndl GJ, Weinbauer MG (2004). Diel cycles in viral infection of bacterioplankton in the North Sea. *Aquat Mircob Ecol 35: 207-216*

Winter C, Moeseneder M, Herndl GJ, Weinbauer M (2008). Relationship of Geographic Distance, Depth, Temperature, and Viruses with Prokaryotic Communities in the Eastern Tropical Atlantic Ocean. *Microb Ecol* 56: 383-389.

Winter C, Weinbauer MG (2010). Randomly Amplified Polymorphic DNA Reveals Tight Links between Viruses and Microbes in the Bathypelagic Zone of the Northwestern Mediterranean Sea. *Appl Environ Microb* 76: 6724-6732.

Winter C, Bouvier T, Weinbauer MG, Thingstad TF (2010). Trade-Offs between Competition and Defense Specialists among Unicellular Planktonic Organisms: the "Killing the Winner" Hypothesis Revisited. *Microbiol Mol Biol R* 74: 42-57.

Wommack KE, Colwell RR (2000). Virioplankton: Viruses in Aquatic Ecosystems. *Microbiol Mol Biol R* 64: 69-114.

Tables

Table 1: Average prokaryotic and viral abundance (N x 10^5 mL^{-1}) in *Experiment 1* of the 7 treatments and the *in-situ* samples.

Treatment	Prokaryotes	STD	Viruses	STD	V/P ratio
MSOW$_{prok}$/MSOW	0.29	0.07	2.94	0.96	10.3
MSOW$_{prok}$/NADW	0.25	0.05	2.33	1.07	9.2
NADW$_{prok}$/MSOW	0.08	0.01	2.59	1.14	32.5
NADW$_{prok}$/NADW	0.09	0.02	1.72	0.69	19.1
MSOW$_{prok}$NADW$_{prok}$/MSOW	0.16	0.03	2.40	0.89	14.8
MSOW$_{prok}$NADW$_{prok}$/NADW	0.18	0.05	1.85	0.88	10.5
MSOW$_{prok}$NADW$_{prok}$/MSOW/NADW	0.17	0.03	2.01	0.94	12.1
Station 2/900 m	0.67	-	15.45	-	23.1
Station 2/2750 m	0.26	-	7.57	-	29.1

Table 2: Average prokaryotic and viral abundance (N x 10^5 mL^{-1}) in *Experiment 2* of the 7 treatments and the *in-situ* samples.

Treatment	Prokaryotes	STD	Viruses	STD	V/P ratio
AAIW$_{prok}$/AAIW	0.15	0.02	1.00	0.39	6.7
AAIW$_{prok}$/NADW	0.15	0.02	0.89	0.48	5.7
NADW$_{prok}$/AAIW	0.08	0.01	1.03	0.43	12.9
NADW$_{prok}$/NADW	0.08	0.01	0.23	0.16	3.0
AAIW$_{prok}$NADW$_{prok}$/AAIW	0.12	0.01	1.13	0.55	9.6
AAIW$_{prok}$NADW$_{prok}$/NADW	0.12	0.01	0.66	0.32	5.6
AAIW$_{prok}$NADW$_{prok}$/AAIW/NADW	0.12	0.01	0.88	0.49	7.3
Station 7/1300 m	0.44	-	7.02	-	16
Station 7/2750 m	0.22	-	5.55	-	25.2

Table 3: Average percentages for each population within prokaryotes and viruses detected via flow cytometry in *Experiment 1*.

Treatment	Prokaryotes (%)		Viruses (%)		
	HNA	LNA	VirLow	VirMed	VirHigh
MSOW$_{prok}$/MSOW	53.4	46.6	70.1	29.2	0.7
MSOW$_{prok}$/NADW	54.1	45.9	70.3	29.1	0.7
NADW$_{prok}$/MSOW	61.8	38.2	74	25.7	0.3
NADW$_{prok}$/NADW	61.3	38.7	74.7	24.8	0.5
MSOW$_{prok}$NADW$_{prok}$/MSOW	54.5	45.5	73.2	26.6	0.2
MSOW$_{prok}$NADW$_{prok}$/NADW	57.7	45.3	68.8	30.1	0.1
MSOW$_{prok}$NADW$_{prok}$/MSOW/NADW	55.2	44.8	69.9	29.4	0.7
Station 2/900 m	56.4	43.6	46.0	49.0	5
Station 2/2750 m	65.3	34.7	30.8	63.7	5.5

Table 4: Average percentages for each population within prokaryotes and viruses detected via flow cytometry in *Experiment 2*.

Treatment	Prokaryotes (%)		Viruses (%)		
	HNA	LNA	VirLow	VirMed	VirHigh
AAIW$_{prok}$/AAIW	61.4	38.6	83.7	14.7	1.6
AAIW$_{prok}$/NADW	60.8	39.2	82.7	15.5	1.8
NADW$_{prok}$/AAIW	56.6	43.4	88.9	10.1	1.0
NADW$_{rok}$/NADW	56.8	43.2	66.4	27.4	6.2
AAIW$_{prok}$NADW$_{prok}$/AAIW	58.9	41.1	85.1	13.7	1.3
AAIW$_{prok}$NADW$_{prok}$/NADW	59.3	40.7	83.1	15.0	1.9
AAIW$_{prok}$NADW$_{prok}$/AAIW/NADW	58.4	41.6	86.5	12.2	1.4
Station 7/1300 m	55.5	44.5	47.8	47.7	4.4
Station 7/2750 m	55.2	44.8	52.0	43.5	4.5

Table 5: Mantel tests (r_M) calculated between bacterial, archaeal, and viral communities as detected by T-RFLP and RAPD-PCR. Only relevant results are shown ($r_M \geq 0.5$) for all possible combinations in *Experiment 1* and *2*.

Experiment 1	Bacteria reverse	Archaea reverse	CRA-22	OPA-13
Bacteria forward	**0.67**	-	-	-
Archaea forward	-	-	-	-
Experiment 2				
Bacteria forward	**0.64**	-	-	-
Archaea forward	-	-	-	-

Table 6: Mantel statistics of bacterial, archaeal, and viral community composition calculated between the duplicates of all treatments; only relevant results are shown ($r_M \geq 0.5$).

	A1 vs B1	A2 vs B2	A3 vs B3	A4 vs B4	A5 vs B5	A6 vs B6	A7 vs B7
Bacteria forward							
Experiment 1	0.5	-	-	-	-	0.9	-
Experiment 2	-	-	-	-	-	-	0.86
Bacteria reverse							
Experiment 1	-	0.94	-	-	-	-	-
Experiment 2	-	-	-	0.78	-	1	-
Archaea forward							
Experiment 1	-	0.98	-	-	0.5	-	-
Experiment 2	-	-	-	-	-	1	-
Archaea reverse							
Experiment 1	-	-	0.9	-	0.69	0.5	0.96
Experiment 2	0.8	0.8	-	0.75	0.69	-	-
CRA-22							
Experiment 1	0.88	-	-	-	-	-	-
Experiment 2	-	-	-	-	-	-	-
OPA-13							
Experiment 1	0.98	-	-	0.98	1	0.98	0.5
Experiment 2	0.93	-	-	-	0.95	0.99	0.99

Table 7: Mantel statistics of bacterial, archaeal, and viral community composition calculated between the treatments of the two experiments; only relevant results are shown ($r_M \geq 0.5$).

Experiment 1 vs *Experiment 2*	Treatment 1	Treatment 2	Treatment 3	Treatment 4	Treatment 5	Treatment 6	Treatment 7
Bacteria forward	-	-	-	0.72	-	-	-
Bacteria reverse	0.52	-	-	-	0.60	-	-
Archaea forward	-	-	-	-	-	-	-
Archaea reverse	-	-	-	-	-	-	-
CRA-22	-	-	-	-	-	-	-
OPA-13	-	-	-	-	-	0.50	0.50

Figures
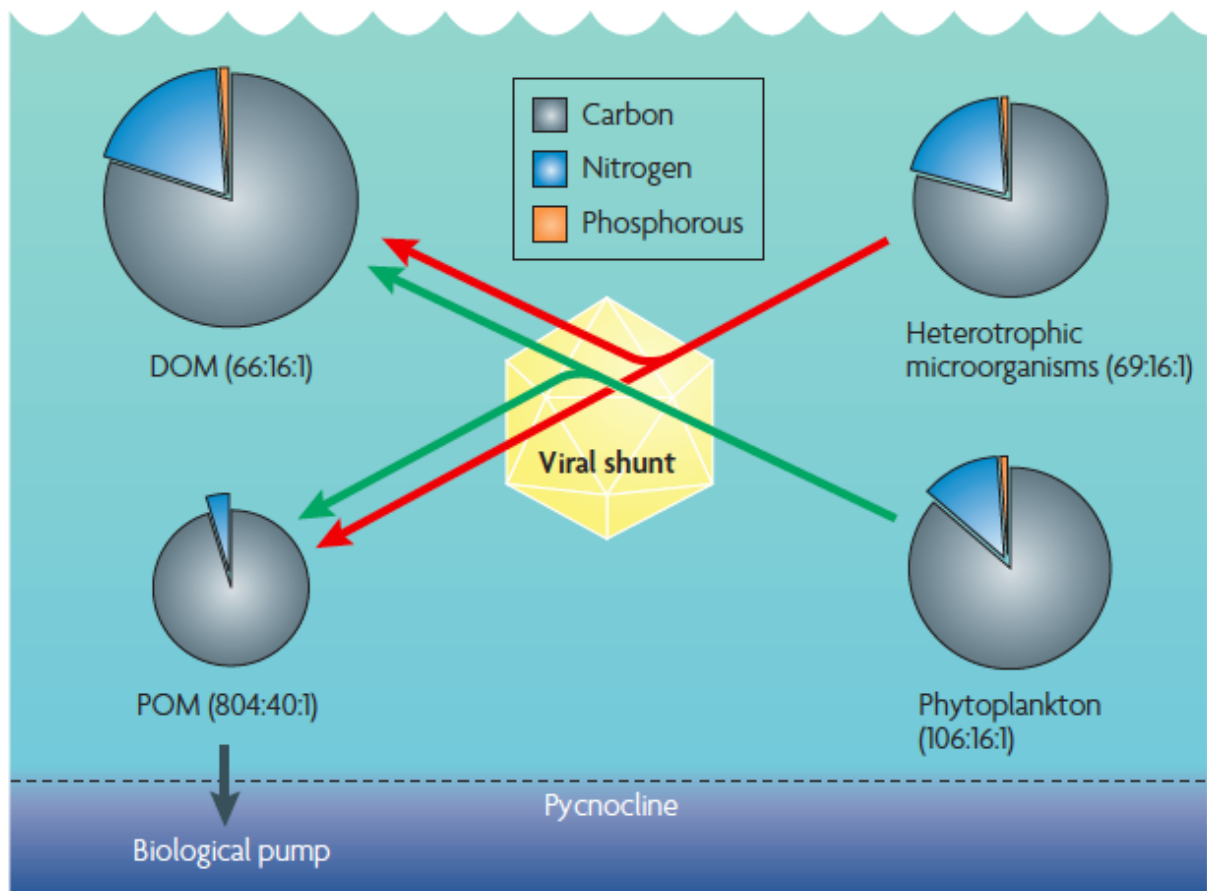
Figure 1: The *viral shunt*. Viruses shunt material from heterotrophic microorganisms and phytoplankton to DOM and POM pools. Labile compounds are recycled within surface waters, whereas more refractory material sinks down via the biological pump (Figure copyright by C.A. Suttle, 2005).
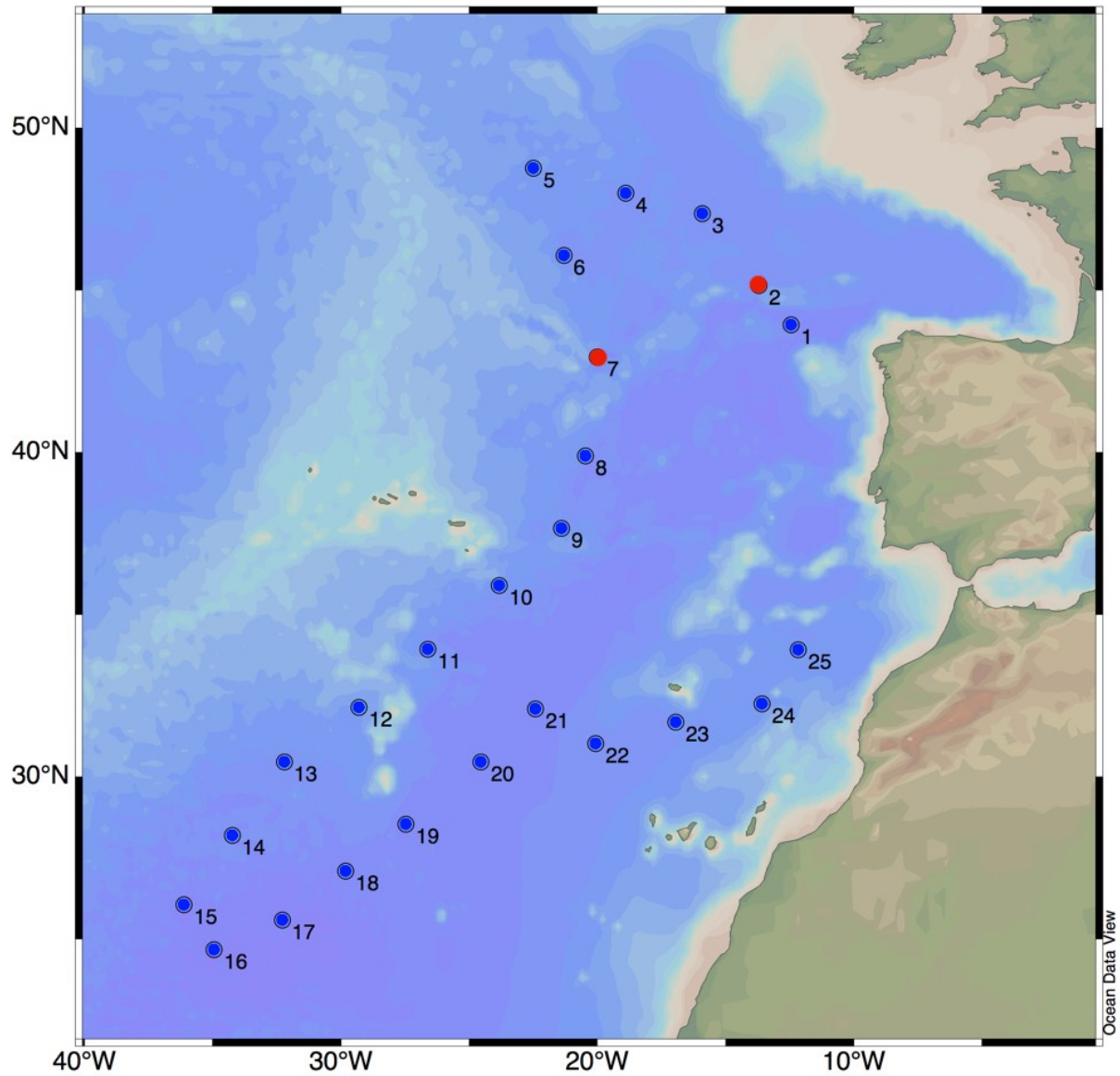
Figure 2: Map of the MEDEA-1 cruise in the North Atlantic Ocean sampled in Oct-Nov 2011; sampling stations are indicated by dots. Samples from 2 and 7 (labeled red) were used for analysis in this study (Figure by Thomas Reinthaler).
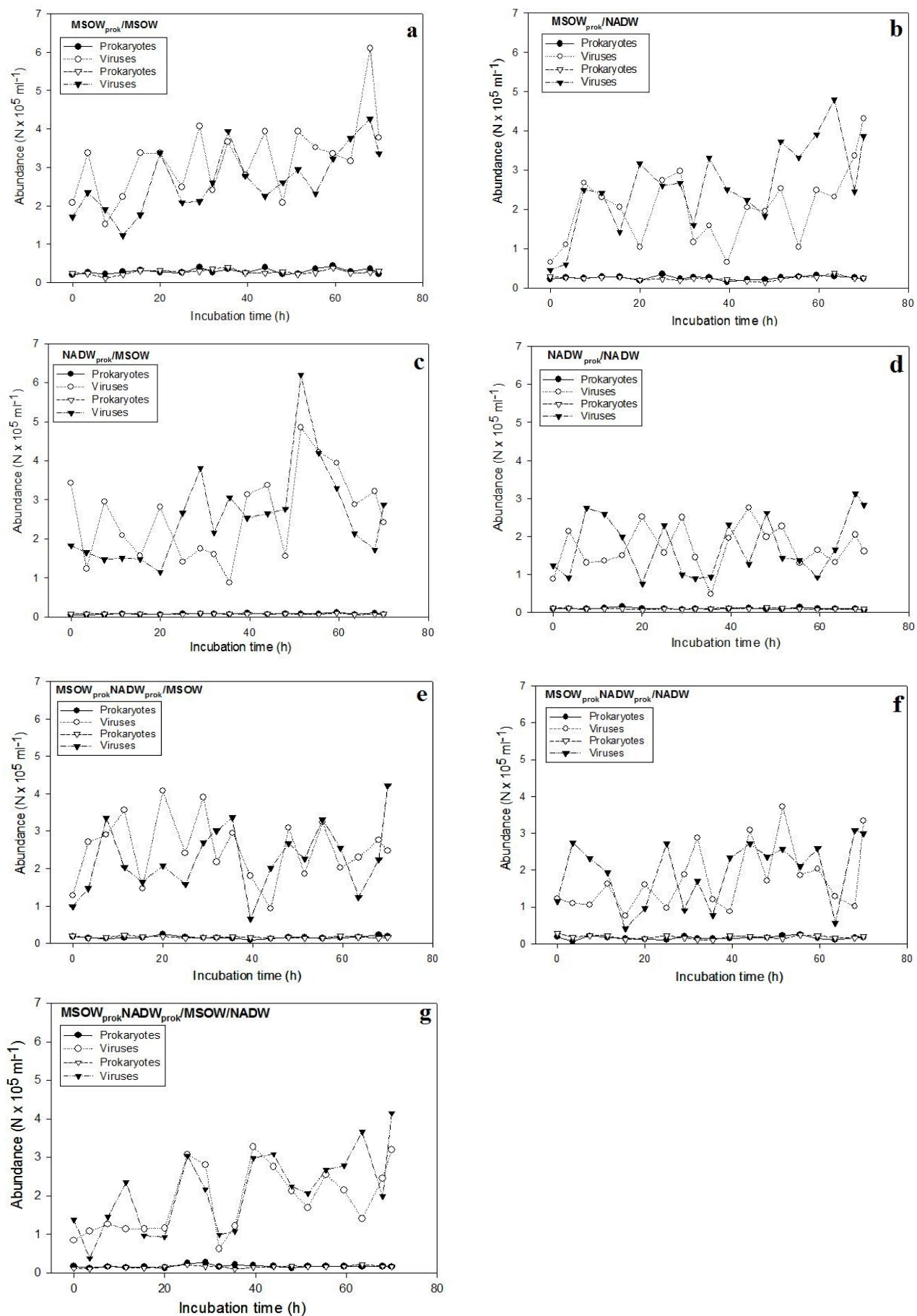
Figure 3: Prokaryotic and viral abundance measured (in duplicates) over an incubation period of 70 h in *Experiment 1*.
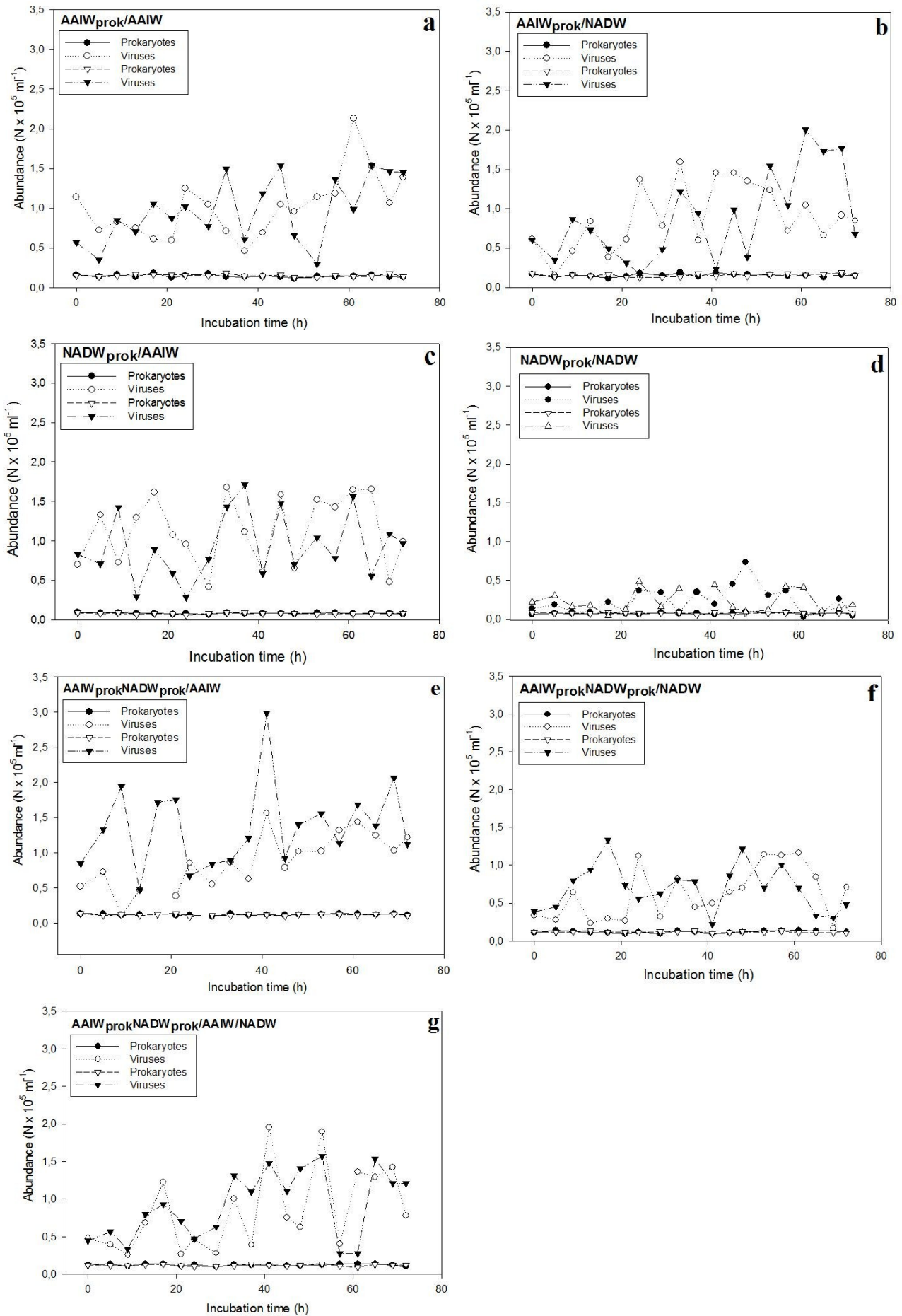
Figure 4: Prokaryotic and viral abundance measured (in duplicates) over an incubation period of 72 h in *Experiment 2*.
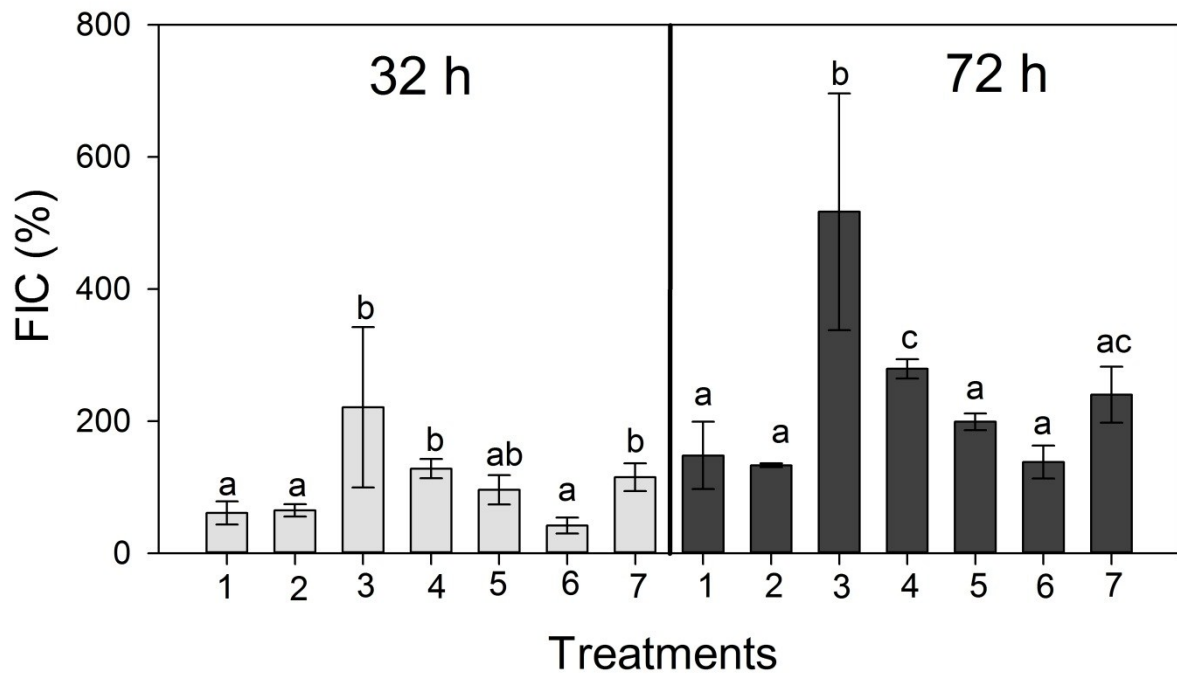
Figure 5: Frequency of infected cells in *Experiment 1* over 32 h and 72 h incubation time. Error bars indicate the range of the duplicates and were arranged to groups (a, b, c) when they overlapped.
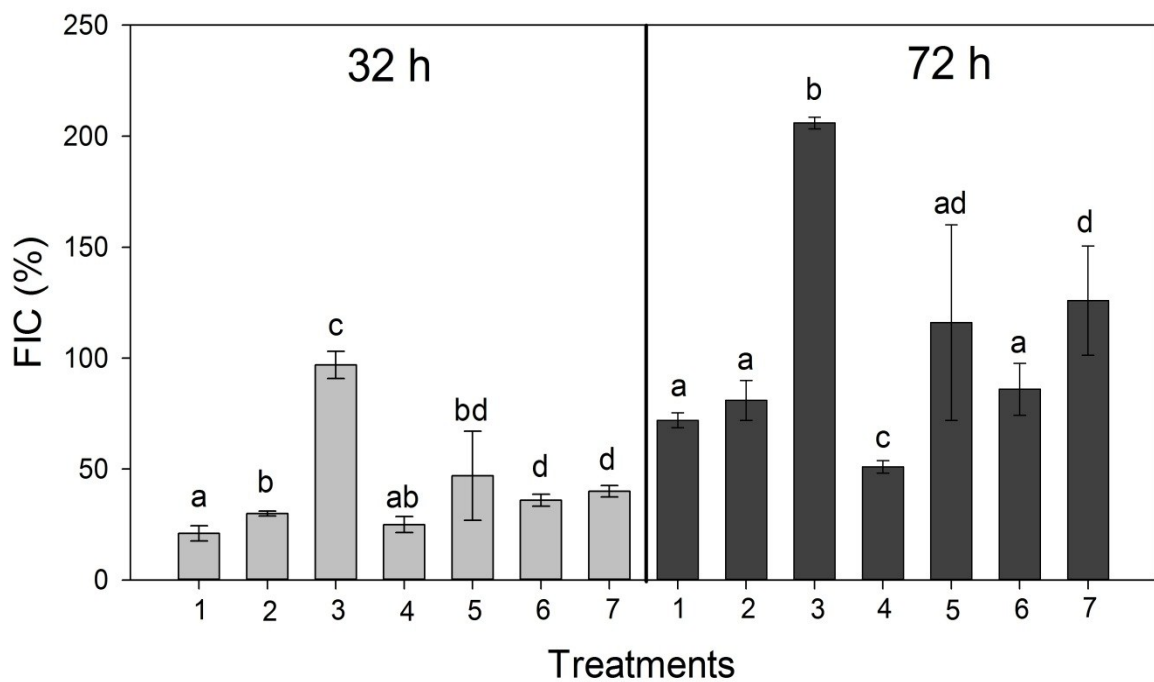
Figure 6: Frequency of infected cells in *Experiment 2* over 32 h and 72 h of incubation time. Error bars indicate the range of the duplicates and were arranged to groups (a, b, c, d) when they overlapped.
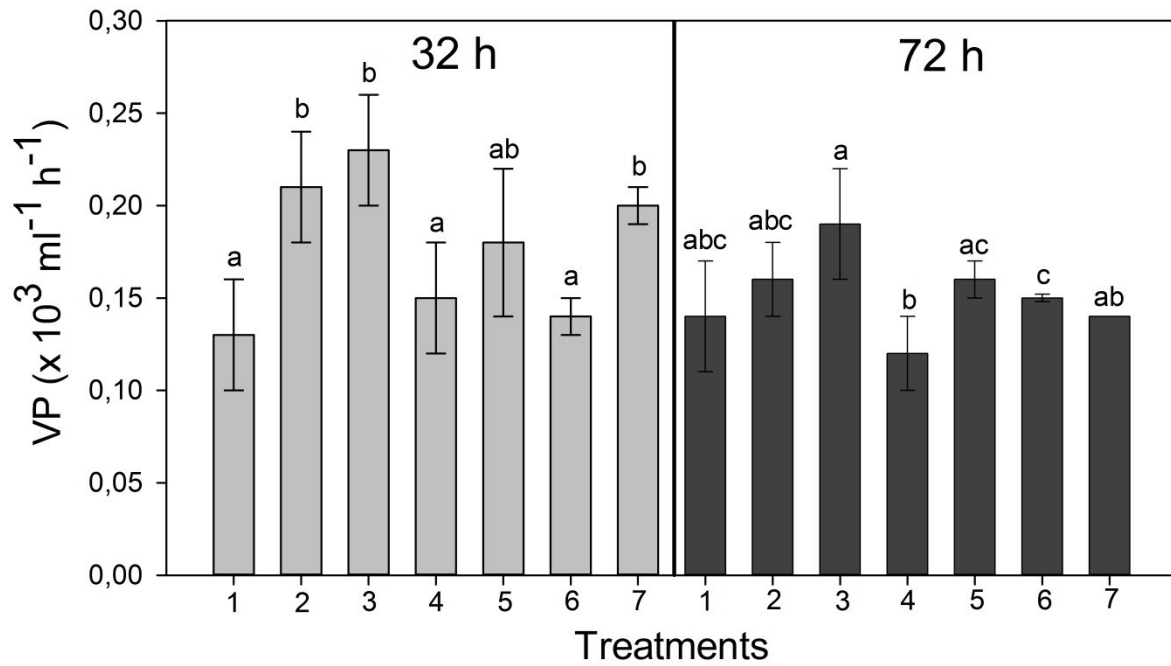
Figure 7: Viral production in *Experiment 1* over 32 h and 72 h of incubation time.
Error bars indicate the range of the duplicates and were arranged to groups (a, b, c) when they overlapped.
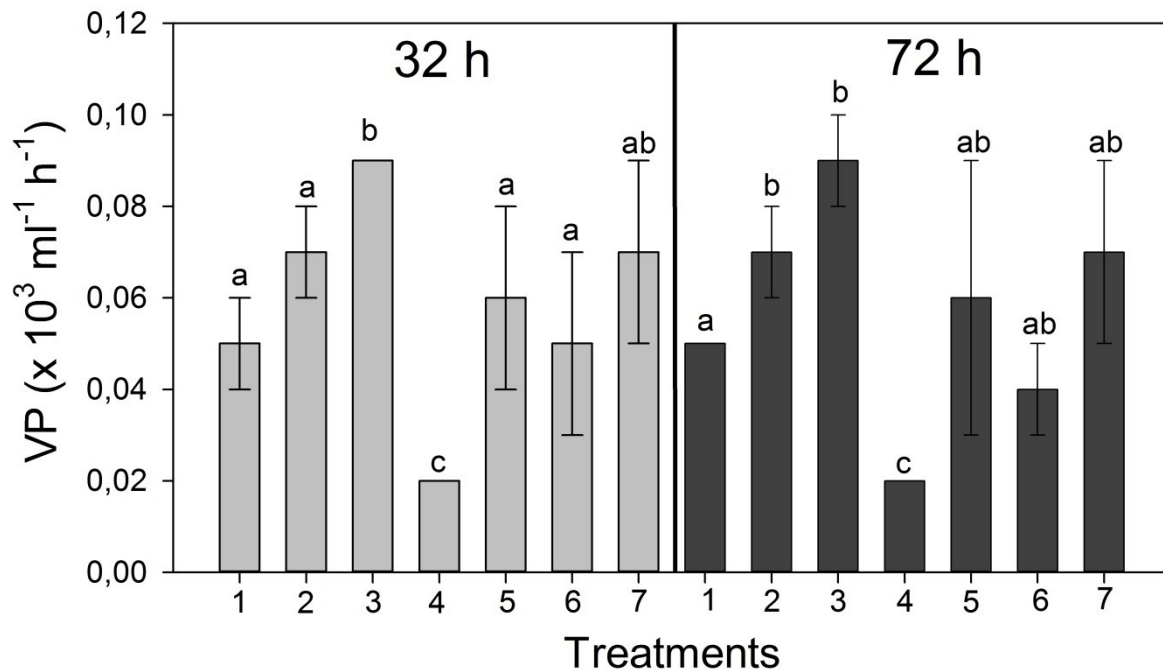
Figure 8: Viral production in *Experiment 2* over 32 h and 72 h of incubation time
Error bars indicate the range of the duplicates and were arranged to groups (a, b, c) when they overlapped
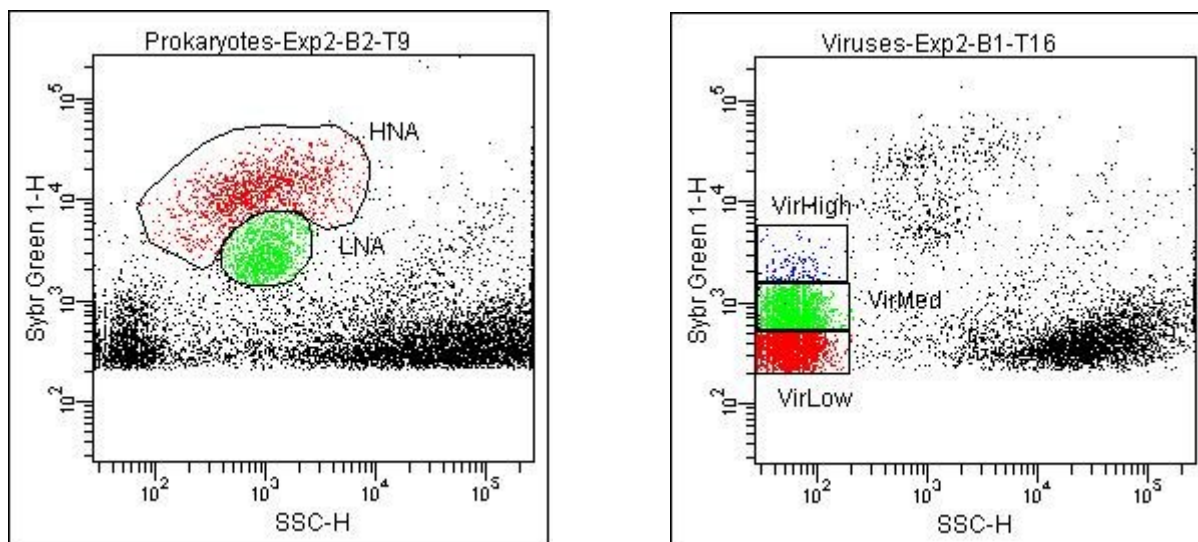
Figure 9: Typical flow cytometric signature of the two prokaryotic populations (left) LNA = low nucleic acid and HNA = high nucleic acid stained with SYBRGreenI and plotted against SSC-H = side scatter – height. On the right side are the three viral populations gated, VirLow, VirMed and VirHigh. The black patches on the far right of both graphs are noise.
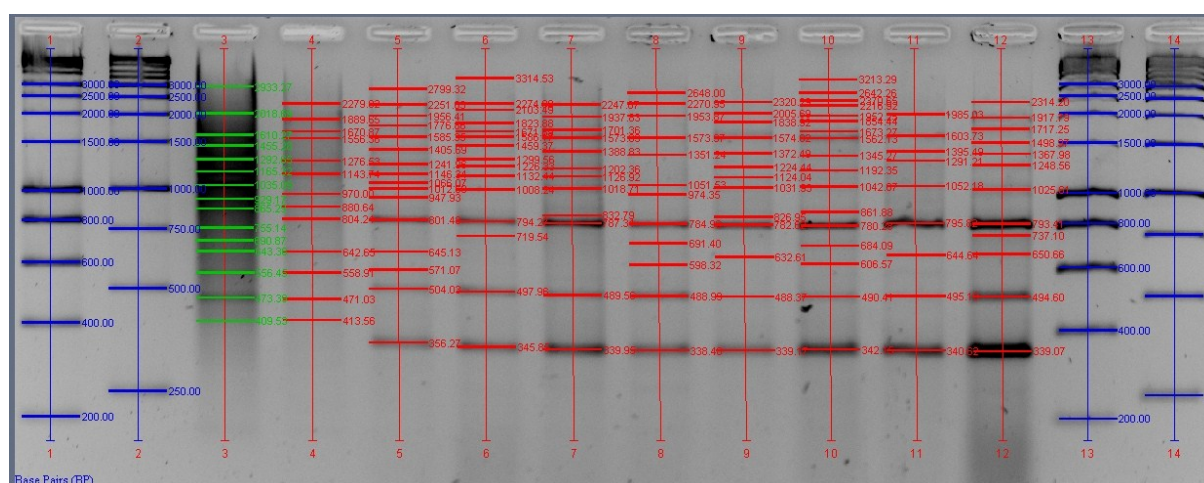
Figure 10: Typical viral banding pattern received from RAPD-PCR (used primer: CRA-22) that was analyzed with GelDoc EQ imaging software to detect the band patterns and their base pairs. The four blue lanes represent the two used size markers, SmartLadder (Lane 1 and 13) and Fermentas gene ruler (Lane 2 and 14). On lane 3 (green) and 4 the *in-situ* samples of *Experiment 2* were applied for comparison. Lane 5 to 12 represent the samples of the seven different treatments. Numbers next to each lane display numbers of base pairs according to the size markers.

Sample Name	Incubation time (h)	Σ of peaks
Exp.1-A1-T6	25	4
Exp.1-B1-T6	25	2
Exp.1-A1-T12	48	5
Exp.1-B1-T12	48	3
Exp.1-A1-T18	70	10
Exp.1-B1-T18	70	18
Exp.1-A2-T6	25	6
Exp.1-B2-T6	25	9
Exp.1-A2-T12	48	5
Exp.1-B2-T12	48	7
Exp.1-A2-T18	70	11
Exp.1-B2-T18	70	14
Exp.1-A3-T6	25	8
Exp.1-B3-T6	25	6
Exp.1-A3-T12	48	6
Exp.1-B3-T12	48	5
Exp.1-A3-T18	70	6
Exp.1-B3-T18	70	4
Exp.1-A4-T6	25	2
Exp.1-B4-T6	25	5
Exp.1-A4-T12	48	4
Exp.1-B4-T12	48	4
Exp.1-A4-T18	70	8
Exp.1-B4-T18	70	4
Exp.1-A5-T6	25	5
Exp.1-B5-T6	25	2
Exp.1-A5-T12	48	4
Exp.1-B5-T12	48	12
Exp.1-A5-T18	70	5
Exp.1-B5-T18	70	6
Exp.1-A6-T6	25	3
Exp.1-B6-T6	25	10
Exp.1-A6-T12	48	15
Exp.1-B6-T12	48	4
Exp.1-A6-T18	70	4
Exp.1-B6-T18	70	8
Exp.1-A7-T6	25	5
Exp.1-B7-T6	25	7
Exp.1-A7-T12	48	8
Exp.1-B7-T12	48	6
Exp.1-A7-T18	70	8
Exp.1-B7-T18	70	5
Station 2/900 m		2
Station 2/2750 m		2

Column headers (fragment sizes): 26, 28, 29, 30, 31, 32, 33, 35, 36, 40, 41, 42, 45, 46, 47, 49, 51, 53, 73, 90, 175, 176, 177, 206, 221, 222, 353, 364, 366, 373, 383, 849, 903, 1050, 1111

Figure 11: Presence/absence (black/white) matrix for the *Experiment 1* of T-RFLP with the forward primer (27 F-FAM) for *Bacteria*.
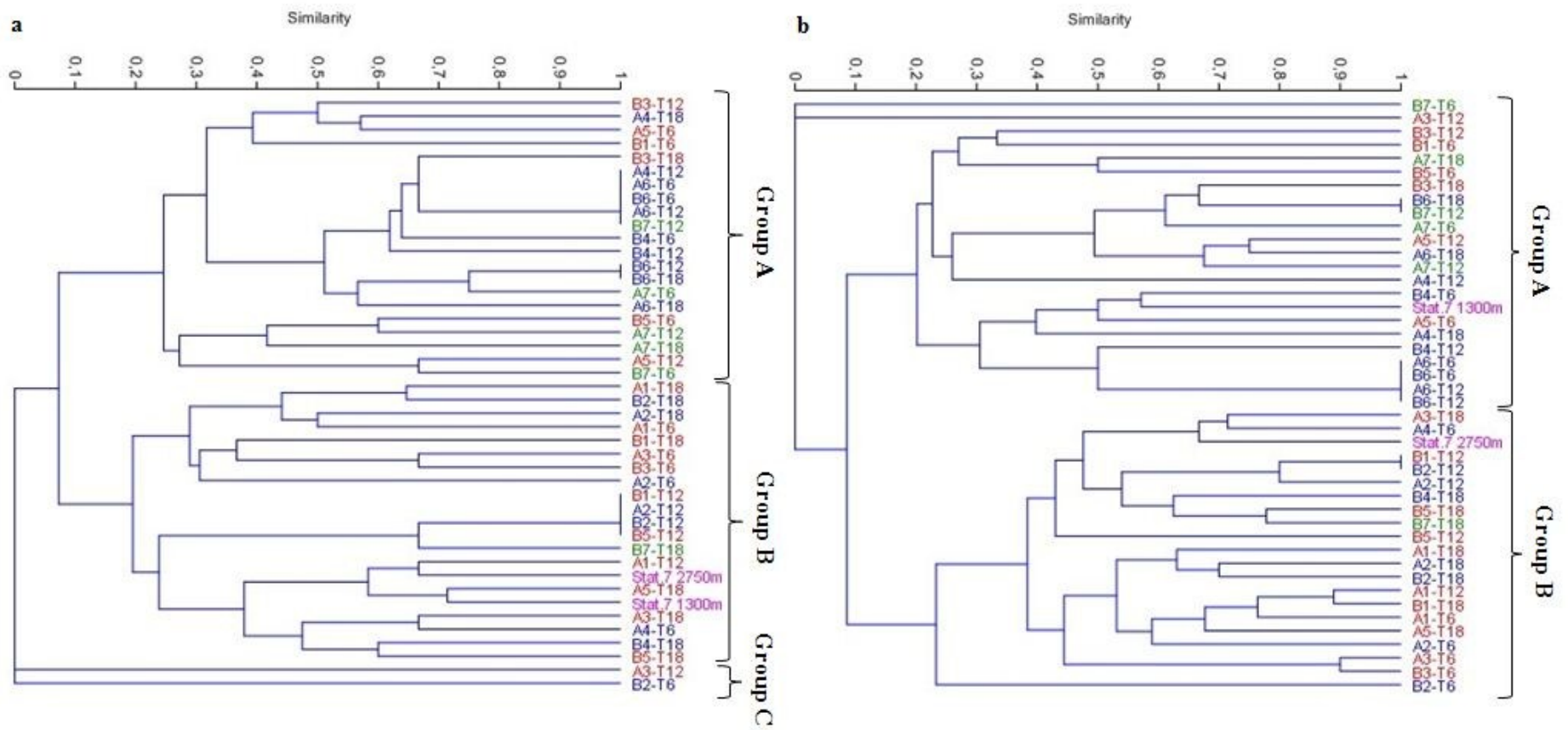
44

Figure 12: Jaccard cluster analysis for the dataset of *Experiment 1* of the forward primer (a) and the reverse primer (b) for *Bacteria*. MSOW is red-labeled; NADW is blue-labeled; MSOW+NADW is green-labeled; *In-situ* samples are purple-labeled.

Sample Name	Incubation Time (h)	Σ of peaks
Exp.1-A1-T6	25	4
Exp.1-B1-T6	25	3
Exp.1-A1-T12	48	8
Exp.1-B1-T12	48	2
Exp.1-A1-T18	70	14
Exp.1-B1-T18	70	20
Exp.1-A2-T6	25	10
Exp.1-B2-T6	25	11
Exp.1-A2-T12	48	9
Exp.1-B2-T12	48	8
Exp.1-A2-T18	70	12
Exp.1-B2-T18	70	17
Exp.1-A3-T6	25	12
Exp.1-B3-T6	25	6
Exp.1-A3-T12	48	4
Exp.1-B3-T12	48	7
Exp.1-A3-T18	70	4
Exp.1-B3-T18	70	4
Exp.1-A4-T6	25	4
Exp.1-B4-T6	25	6
Exp.1-A4-T12	48	3
Exp.1-B4-T12	48	3
Exp.1-A4-T18	70	10
Exp.1-B4-T18	70	6
Exp.1-A5-T6	25	8
Exp.1-B5-T6	25	2
Exp.1-A5-T12	48	5
Exp.1-B5-T12	48	20
Exp.1-A5-T18	70	11
Exp.1-B5-T18	70	11
Exp.1-A6-T6	25	6
Exp.1-B6-T6	25	13
Exp.1-A6-T12	48	18
Exp.1-B6-T12	48	6
Exp.1-A6-T18	70	3
Exp.1-B6-T18	70	14
Exp.1-A7-T6	25	7
Exp.1-B7-T6	25	8
Exp.1-A7-T12	48	11
Exp.1-B7-T12	48	5
Exp.1-A7-T18	70	12
Exp.1-B7-T18	70	6
Station 2/900 m		5
Station 2/2750 m		5

Peak columns: 28, 29, 30, 31, 32, 33, 34, 35, 36, 38, 39, 42, 43, 44, 45, 46, 47, 49, 50, 51, 52, 53, 55, 63, 64, 73, 80, 110, 133, 134, 135, 136, 140, 141, 143, 242, 375, 389, 394, 398, 400, 401, 402, 403, 406, 527

Figure 13: Presence/absence (black/white) matrix for the dataset of *Experiment 1* of T-RFLP with the reverse primer (1492 R-VIC) for *Bacteria*.

Sample Name	Incubation time (h)	Σ of peaks
Exp.2-A1-T6	24	6
Exp.2-B1-T6	24	9
Exp.2-A1-T12	48	6
Exp.2-B1-T12	48	2
Exp.2-A1-T18	72	12
Exp.2-B1-T18	72	8
Exp.2-A2-T6	24	4
Exp.2-B2-T6	24	0
Exp.2-A2-T12	48	2
Exp.2-B2-T12	48	2
Exp.2-A2-T18	72	9
Exp.2-B2-T18	72	16
Exp.2-A3-T6	24	6
Exp.2-B3-T6	24	4
Exp.2-A3-T12	48	0
Exp.2-B3-T12	48	8
Exp.2-A3-T18	72	3
Exp.2-B3-T18	72	3
Exp.2-A4-T6	24	2
Exp.2-B4-T6	24	3
Exp.2-A4-T12	48	2
Exp.2-B4-T12	48	3
Exp.2-A4-T18	72	6
Exp.2-B4-T18	72	3
Exp.2-A5-T6	24	5
Exp.2-B5-T6	24	3
Exp.2-A5-T12	48	3
Exp.2-B5-T12	48	2
Exp.2-A5-T18	72	6
Exp.2-B5-T18	72	5
Exp.2-A6-T6	24	2
Exp.2-B6-T6	24	2
Exp.2-A6-T12	48	2
Exp.2-B6-T12	48	3
Exp.2-A6-T18	72	5
Exp.2-B6-T18	72	3
Exp.2-A7-T6	24	4
Exp.2-B7-T6	24	2
Exp.2-A7-T12	48	5
Exp.2-B7-T12	48	2
Exp.2-A7-T18	72	3
Exp.2-B7-T18	72	3
Station 7/1300 m		6
Station 7/2750 m		4

Matrix columns (T-RF sizes): 22, 25, 26, 27, 28, 29, 30, 31, 32, 33, 34, 35, 36, 38, 63, 90, 175, 176, 177, 220, 221, 363, 366, 372, 374, 383, 559, 567, 850, 903, 1050, 1053

Figure 14: Presence/absence (black/white) matrix for the dataset of *Experiment 2* of T-RFLP with the forward primer (27 F-FAM) for *Bacteria*.

Figure 15: Jaccard cluster analysis for the dataset of *Experiment 2* of the forward primer (a) and the reverse primer (b) for *Bacteria*. AAIW is red-labeled; NADW is blue-labeled; AAIW+NADW is green-labeled; *In-situ* samples are purple-labeled.

Figure 16: Presence/absence (black/white) matrix for the dataset of *Experiment 2* of T-RFLP with the reverse primer (1492 R-VIC) for *Bacteria*.

Sample Name	Incubation Time (h)	Σ of peaks	27	28	29	30	33	322	331	585	913
Exp.1-A1-T6	25	1						■			
Exp.1-B1-T6	25	4			■	■		■			■
Exp.1-A1-T12	48	2		■				■			
Exp.1-B1-T12	48	6			■	■		■	■	■	■
Exp.1-A1-T18	70	4		■					■	■	■
Exp.1-B1-T18	70	1						■			
Exp.1-A2-T6	25	2		■				■			
Exp.1-B2-T6	25	5		■		■		■		■	■
Exp.1-A2-T12	48	3	■	■				■			
Exp.1-B2-T12	48	6				■	■	■	■	■	■
Exp.1-A2-T18	70	3						■		■	■
Exp.1-B2-T18	70	2				■		■			
Exp.1-A3-T6	25	3		■			■	■			
Exp.1-B3-T6	25	2		■				■			
Exp.1-A3-T12	48	1		■							
Exp.1-B3-T12	48	2						■			■
Exp.1-A3-T18	70	1						■			
Exp.1-B3-T18	70	1						■			
Exp.1-A4-T6	25	1						■			
Exp.1-B4-T6	25	1						■			
Exp.1-A4-T12	48	2		■				■			
Exp.1-B4-T12	48	1						■			
Exp.1-A4-T18	70	3			■	■		■			
Exp.1-B4-T18	70	1						■			
Exp.1-A5-T6	25	1						■			
Exp.1-B5-T6	25	1						■			
Exp.1-A5-T12	48	2					■	■			
Exp.1-B5-T12	48	3						■		■	■
Exp.1-A5-T18	70	2						■		■	
Exp.1-B5-T18	70	1						■			
Exp.1-A6-T6	25	1						■			
Exp.1-B6-T6	25	1						■			
Exp.1-A6-T12	48	1						■			
Exp.1-B6-T12	48	4		■				■		■	■
Exp.1-A6-T18	70	2						■		■	
Exp.1-B6-T18	70	1						■			
Exp.1-A7-T6	25	1						■			
Exp.1-B7-T6	25	3		■				■		■	
Exp.1-A7-T12	48	1						■			
Exp.1-B7-T12	48	1						■			
Exp.1-A7-T18	70	3						■		■	■
Exp.1-B7-T18	70	6		■		■	■	■		■	■
Station 2/900 m		4						■		■	■
Station 2/2750 m		2						■	■		

Figure 17: Presence/absence (black/white) matrix for the dataset of *Experiment 1* of T-RFLP with the forward primer (21 F-FAM) for *Archaea*.
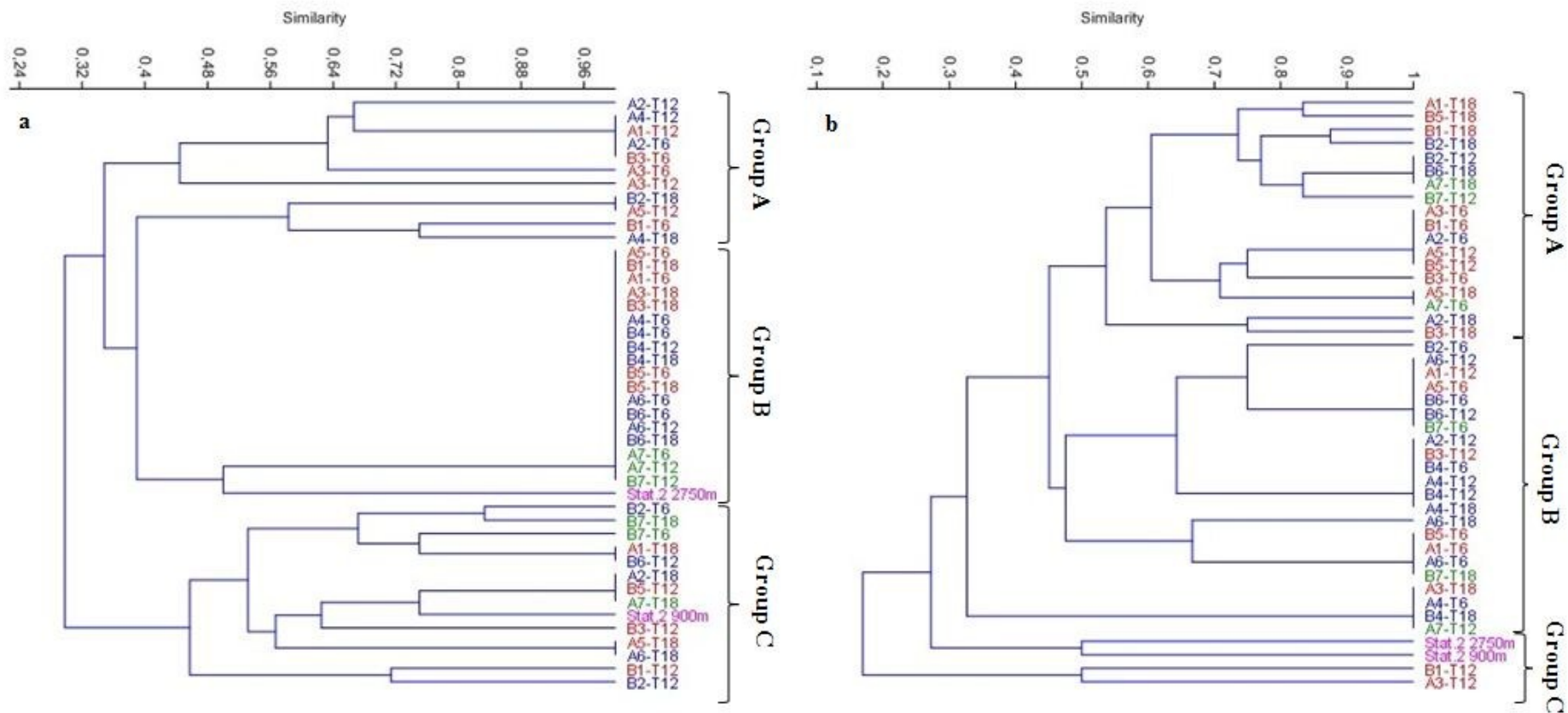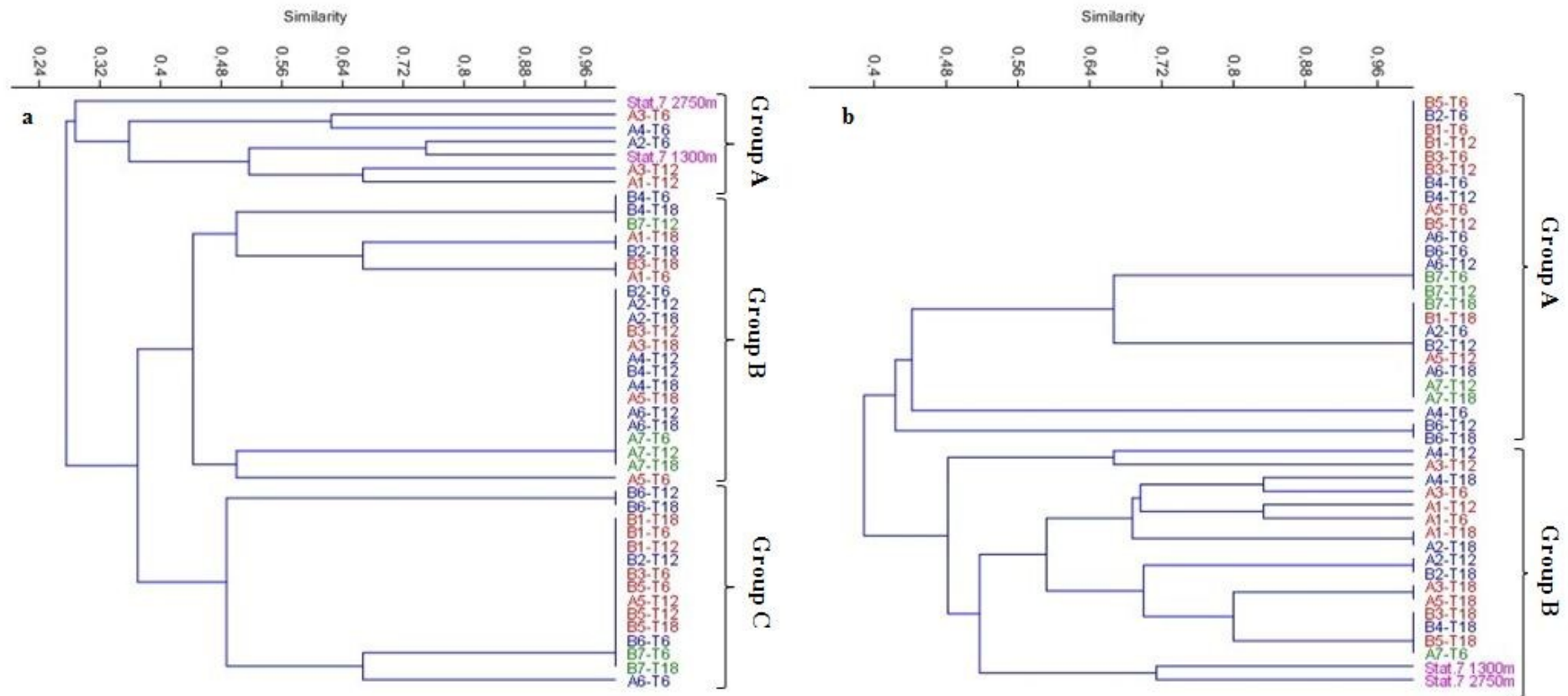
Figure 18: Jaccard cluster analysis for the dataset of *Experiment 1* of the forward primer (a) and the reverse primer (b) for *Archaea*. MSOW is red-labeled; NADW is blue-labeled; MSOW+NADW is green-labeled; *In-situ* samples are purple-labeled.

Sample Name	Incubation Time (h)	Σ of peaks	29	129	232	247	322	363	436	586	869	914
Exp.1-A1-T6	25	2										
Exp.1-B1-T6	25	4										
Exp.1-A1-T12	48	3										
Exp.1-B1-T12	48	2										
Exp.1-A1-T18	70	6										
Exp.1-B1-T18	70	8										
Exp.1-A2-T6	25	4										
Exp.1-B2-T6	25	4										
Exp.1-A2-T12	48	2										
Exp.1-B2-T12	48	6										
Exp.1-A2-T18	70	4										
Exp.1-B2-T18	70	7										
Exp.1-A3-T6	25	4										
Exp.1-B3-T6	25	3										
Exp.1-A3-T12	48	1										
Exp.1-B3-T12	48	2										
Exp.1-A3-T18	70	1										
Exp.1-B3-T18	70	3										
Exp.1-A4-T6	25	1										
Exp.1-B4-T6	25	2										
Exp.1-A4-T12	48	2										
Exp.1-B4-T12	48	2										
Exp.1-A4-T18	70	2										
Exp.1-B4-T18	70	1										
Exp.1-A5-T6	25	3										
Exp.1-B5-T6	25	2										
Exp.1-A5-T12	48	4										
Exp.1-B5-T12	48	4										
Exp.1-A5-T18	70	3										
Exp.1-B5-T18	70	5										
Exp.1-A6-T6	25	2										
Exp.1-B6-T6	25	3										
Exp.1-A6-T12	48	3										
Exp.1-B6-T12	48	3										
Exp.1-A6-T18	70	3										
Exp.1-B6-T18	70	6										
Exp.1-A7-T6	25	3										
Exp.1-B7-T6	25	3										
Exp.1-A7-T12	48	1										
Exp.1-B7-T12	48	5										
Exp.1-A7-T18	70	6										
Exp.1-B7-T18	70	2										
Station 2/900 m		6										
Station 2/2750 m		3										

Figure 19: Presence/absence (black/white) matrix for the dataset of *Experiment 1* of T-RFLP with the reverse primer (958 R-VIC) for *Archaea*.

Sample Name	Incubation Time (h)	Σ of peaks	27	28	29	30	33	322	331	585	586	913
Exp.2-A1-T6	24	3			■			■				■
Exp.2-B1-T6	24	2		■				■				
Exp.2-A1-T12	48	3		■				■		■		
Exp.2-B1-T12	48	2		■				■				
Exp.2-A1-T18	72	2						■				■
Exp.2-B1-T18	72	2		■				■				
Exp.2-A2-T6	24	4						■	■			■
Exp.2-B2-T6	24	1						■				
Exp.2-A2-T12	48	1						■				
Exp.2-B2-T12	48	2		■				■				
Exp.2-A2-T18	72	1						■				
Exp.2-B2-T18	72	2						■				■
Exp.2-A3-T6	24	7			■	■	■	■	■			■
Exp.2-B3-T6	24	2		■				■				
Exp.2-A3-T12	48	2						■		■		
Exp.2-B3-T12	48	1						■				
Exp.2-A3-T18	72	1						■				
Exp.2-B3-T18	72	3			■			■				■
Exp.2-A4-T6	24	6			■	■		■		■	■	■
Exp.2-B4-T6	24	2			■			■				
Exp.2-A4-T12	48	1						■				
Exp.2-B4-T12	48	1						■				
Exp.2-A4-T18	72	1						■				
Exp.2-B4-T18	72	2			■			■				
Exp.2-A5-T6	24	2						■			■	
Exp.2-B5-T6	24	2		■				■				
Exp.2-A5-T12	48	2		■				■				
Exp.2-B5-T12	48	2		■				■				
Exp.2-A5-T18	72	1						■				
Exp.2-B5-T18	72	2		■				■				
Exp.2-A6-T6	24	3		■				■				■
Exp.2-B6-T6	24	2		■				■				
Exp.2-A6-T12	48	1						■				
Exp.2-B6-T12	48	1		■								
Exp.2-A6-T18	72	1						■				
Exp.2-B6-T18	72	1		■								
Exp.2-A7-T6	24	1						■				
Exp.2-B7-T6	24	2		■				■				
Exp.2-A7-T12	48	1						■				
Exp.2-B7-T12	48	2				■		■				
Exp.2-A7-T18	72	1						■				
Exp.2-B7-T18	72	2		■				■				
Station 7/1300 m		3						■	■	■		
Station 7/2750 m		3	■					■		■		

Figure 20: Presence/absence (black/white) matrix for the dataset of *Experiment 2* of T-RFLP with the forward primer (21 F-FAM) for *Archaea*.
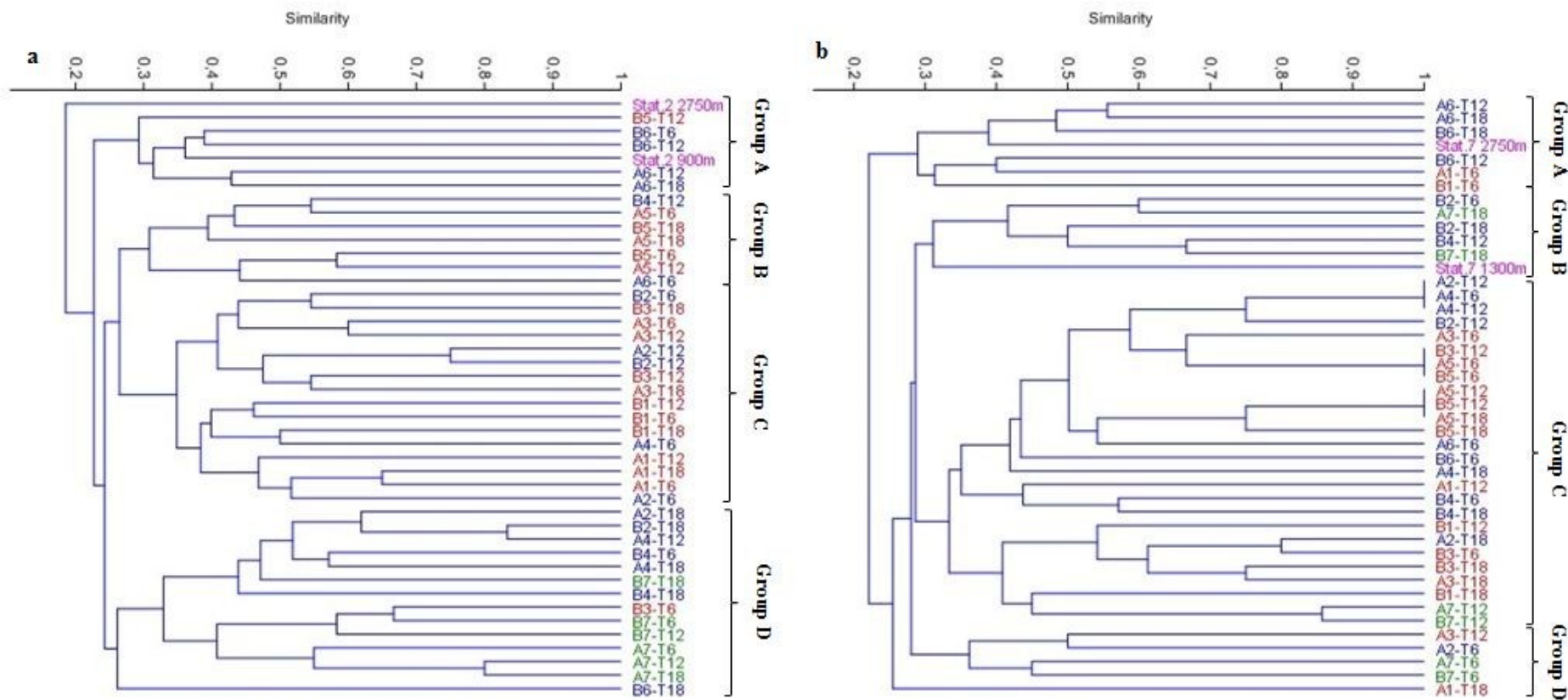
Figure 21: Jaccard cluster analysis for the dataset of *Experiment 2* of the forward primer (a) and the reverse primer (b) for *Archaea*. AAIW is red-labeled; NADW is blue-labeled; AAIW+NADW is green-labeled; *In-situ* samples are purple-labeled.

Sample Name	Incubation Time (h)	Σ of peaks	29	129	232	247	322	363	437	586	869	914
Exp.2-A1-T6	24	5										
Exp.2-B1-T6	24	2										
Exp.2-A1-T12	48	6										
Exp.2-B1-T12	48	2										
Exp.2-A1-T18	72	8										
Exp.2-B1-T18	72	3										
Exp.2-A2-T6	24	3										
Exp.2-B2-T6	24	2										
Exp.2-A2-T12	48	3										
Exp.2-B2-T12	48	3										
Exp.2-A2-T18	72	8										
Exp.2-B2-T18	72	3										
Exp.2-A3-T6	24	6										
Exp.2-B3-T6	24	2										
Exp.2-A3-T12	48	3										
Exp.2-B3-T12	48	2										
Exp.2-A3-T18	72	5										
Exp.2-B3-T18	72	4										
Exp.2-A4-T6	24	1										
Exp.2-B4-T6	24	2										
Exp.2-A4-T12	48	2										
Exp.2-B4-T12	48	2										
Exp.2-A4-T18	72	5										
Exp.2-B4-T18	72	4										
Exp.2-A5-T6	24	2										
Exp.2-B5-T6	24	2										
Exp.2-A5-T12	48	3										
Exp.2-B5-T12	48	2										
Exp.2-A5-T18	72	5										
Exp.2-B5-T18	72	4										
Exp.2-A6-T6	24	2										
Exp.2-B6-T6	24	2										
Exp.2-A6-T12	48	2										
Exp.2-B6-T12	48	1										
Exp.2-A6-T18	72	3										
Exp.2-B6-T18	72	1										
Exp.2-A7-T6	24	4										
Exp.2-B7-T6	24	2										
Exp.2-A7-T12	48	3										
Exp.2-B7-T12	48	2										
Exp.2-A7-T18	72	3										
Exp.2-B7-T18	72	3										
Station 7/1300 m		5										
Station 7/2750 m		7										

Figure 22: Presence/absence (black/white) matrix for the dataset of *Experiment 2* of T-RFLP with the reverse primer (958 F-FAM) for *Archaea*.

Figure 23: Presence/absence matrix for viral community composition received from RAPD-PCR (applied primer CRA-22) for *Experiment 1*.

The numbers in the headline represent the number of basepairs. Black cells = present, white cells = absent.
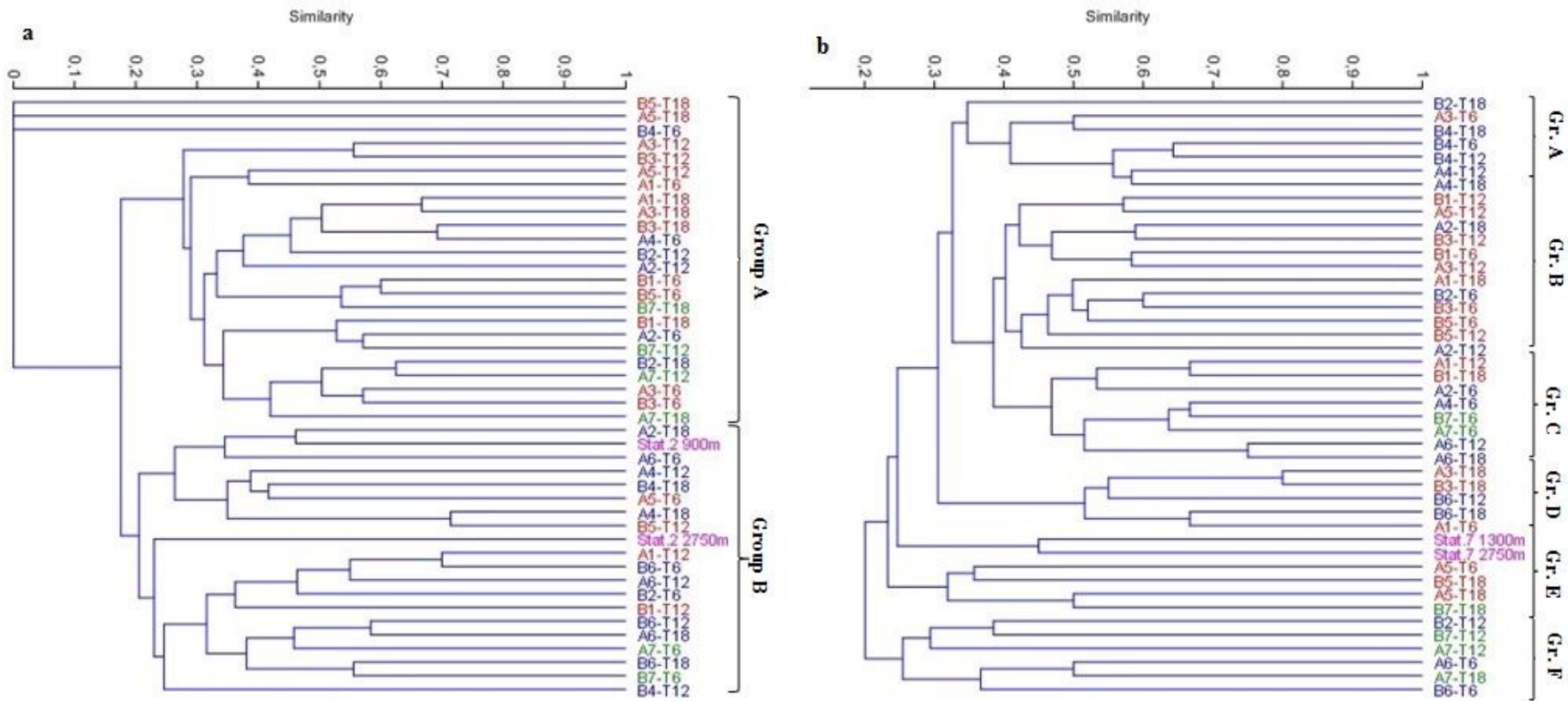
Figure 24: Jaccard cluster analysis for the dataset of *Experiment 1* (a) and *Experiment 2* (b) of the primer CRA-22 for Viruses. MSOW in *Experiment 1* and AAIW in *Experiment 2* are red-labeled; NADW is blue-labeled; MSOW+NADW (AAIW+NADW) is green-labeled; *In-situ* samples are purple-labeled.

Figure 25: Presence/absence matrix for viral community composition received from RAPD-PCR (applied primer CRA-22) for *Experiment 2*.

The numbers in the headline represent the number of basepairs.

Figure 26: Presence/absence matrix of *Experiment 1* conducted for viral community composition RAPD-PCR performed with the primer OPA-13. Black cells represent present basepairs, whereas white cells represent lacking basepairs.

Figure 27: Jaccard cluster analysis for the dataset of *Experiment 1* (a) and *Experiment 2* (b) of the primer OPA-13 for Viruses. MSOW in *Experiment 1* and AAIW in *Experiment 2* are red-labeled; NADW is blue-labeled; MSOW+NADW (AAIW+NADW) is green-labeled; *In-situ* samples are purple-labeled.

Figure 28: Presence/absence matrix of *Experiment 2* conducted for viral community composition RAPD-PCR performed with the primer OPA-13. Black cells represent present basepairs, whereas white cells represent lacking basepairs.

Zusammenfassung

In dieser Studie wurden die Virenproduktion (VP), frequency of infected cells (FIC) und die Zusammensetzung prokaryotischer und viraler Gemeinschaften in zwei Inkubationsexperimenten erhoben. Zahlen zu Abundanzen von Prokaryoten und Viren wurden mittels Durchflusszytometrie erhoben. Diese Methode lässt auch Rückschlüsse auf VP und FIC zu. Mit Hilfe molekularbiologischer Methoden, wie terminal restriction fragment length polymorphism (T-RFLP) und randomly amplified polymorphic DNA Polymerase-Kettenreaktion (RAPD-PCR) wurden die Zusammensetzungen der Prokaryoten- und der Viren-Gemeinschaften festgestellt. Um Zusammenhänge zwischen den Experimenten und deren Mischung aus den verschiedenen Wassermassen aufzuzeigen, wurden Mantel-Tests durchgeführt. Die höchsten Werte für VP und FIC wurden jeweils für Prokaryoten aus dem North Atlantic Deep Water (NADW) beider Experimente errechnet, wenn diese in Wasser aus Mediterranean Sea Overflow Water (MSOW) und Antarctic Intermediate Water (AAIW) inkubiert wurden. Die Werte unterschieden sich signifikant zu den Kontrollproben, was sehr wahrscheinlich auf lysogene Viren zurückzuführen war, die die Prokaryoten des NADW vor Beginn des Experiments bereits infiziert hatten. Das Mischen von Prokaryoten aus dem NADW mit Wasser des MSOW im ersten, bzw. AAIW im zweiten Experiment und die damit hervorgerufene Umweltveränderung, bewirkte wahrscheinlich den Übergang vom lytischen zum lysogenen Zyklus der Viren. Übereinstimmungen in den Gemeinschaften von *Bacteria*, *Archaea* und Viren zwischen den Duplikaten der Inkubationen wurden mittel Mantel Tests ermittelt. Das Fehlen von Übereinstimmungen zwischen den Duplikaten kann als das Überwiegen stochastischer Effekte gedeutet werden. Die Resultate zeigen daher, dass *Archaea*, wenn die Gemeinschaftsstruktur mit dem reversen Primer ermittelt wird, relativ stark durch die experimentellen Manipulationen beeinflusst wurden, wohingegen die Daten der Gemeinschaft der *Bacteria* auf starken Einfluss von stochastischen Effekten hindeuten. Zusätzlich zeigen die Daten zur viralen Gemeinschaftsstruktur, dass Viren, welche mit dem

Primer OPA-13 detektierbar sind, durch die experimentellen Inkubationen viel stärker beeinflusst wurden als Viren, welche mit dem Primer CRA-22 erfasst werden.

Lebenslauf

Carl Philip Kruspe

Geburtsdatum	4. März 1984
Geburtsort	Freudenstadt
Nationalität	deutsch
Familienstand	ledig, keine Kinder

Ausbildung

seit Oktober 2010	Masterstudent der Ökologie/Meeresbiologie
	Universität Wien
01. Oktober 2010	Abschluss als **Bachelor of Science**
	Universität Wien
	• Bachelor-Thesis: Fluoreszenz-in-situ-Hybridisierung – Identifizierung nicht-kultivierter Mikroorganismen
10/2007 bis 10/2010	Studium der Biologie
	Universität Wien
	• Schwerpunkt Ökologie
04/2005 bis 07/2007	Studium der Geschichte und Rechtswissenschaften
	Universität Tübingen
30. Juni 2003	**Abitur**
	Albertus-Magnus-Gymnasium, Rottweil

Praktika

06/2011 bis 07/2011	**IPY-Field-School**
	University centre in Svalbard, Spitzbergen
07/2010	**AWI Wattenmeerstation Sylt**
	Geomorphologie heimischer Fische
07/2007 bis 08/2007	Zivildienst **Kreiskrankenhaus Rottweil**
	Bereich Pflegestation, Labor, Zentralapotheke
12/2004 bis 03/2005	Auslandsaufenthalt in Australien

Sprachen

Englisch	sehr gut
	IELTS-Test

Freizeit

Squash, Reiten, Tauchen, Reisen